Electroceutically induced subthalamic high frequency oscillations and evoked compound activity may explain the mechanism of therapeutic stimulation in Parkinson's Disease

Musa Ozturk
University of Houston
Ashwin Viswanathan
Baylor College of Medicine
Sameer Sheth
Baylor College of Medicine
Nuri Ince (nfince@uh.edu)
University of Houston https://orcid.org/0000-0003-4985-4528

Article

Keywords: Parkinson's Disease, Subthalamic Nucleus, Local Field Potentials, High-frequency Oscillations

Posted Date: October 8th, 2020

DOI: https://doi.org/10.21203/rs.3.rs-63781/v1

Version of Record: A version of this preprint was published at Communications Biology on March 23rd, 2021. See the published version at https://doi.org/10.1038/s42003-021-01915-7.

Electroceutically induced subthalamic high-frequency oscillations and evoked compound activity may explain the mechanism of therapeutic stimulation in Parkinson's disease

Musa Ozturk[1], Ashwin Viswanathan[2], Sameer A. Sheth[2], Nuri F. Ince[1*]

[1]Department of Biomedical Engineering, University of Houston, Houston, TX, USA

[2]Department of Neurosurgery, Baylor College of Medicine Houston, TX, USA

***** Correspondence: nfince@uh.edu

Keywords: Parkinson's Disease, Subthalamic Nucleus, Local Field Potentials, High-frequency Oscillations

Running title: Therapeutic DBS promotes HFO

Abstract

Despite having remarkable utility in treating movement disorders, the lack of understanding of the underlying mechanisms of high-frequency deep brain stimulation (DBS) is a main challenge in choosing personalized stimulation parameters. Here we investigate the modulations in local field potentials induced by therapeutic and non-therapeutic electrical stimulation of the subthalamic nucleus (STN) in Parkinson's disease patients undergoing DBS surgery.

We find that therapeutic high-frequency stimulation (130-180 Hz) induces high-frequency oscillations (~300 Hz, HFO) similar to those observed with pharmacological treatment. Along with HFOs, we also observed evoked compound activity (ECA) after each stimulation pulse. While ECA was observed in both therapeutic and non-therapeutic (20Hz) stimulation, the HFOs were induced only with therapeutic frequencies and the associated ECA were significantly more resonant. The relative degree of enhancement in the HFO power was related to the interaction of stimulation pulse with the phase of ECA.

We propose that high-frequency STN-DBS tunes the neural oscillations to their healthy/treated state, similar to pharmacological treatment, and the stimulation frequency to maximize these oscillations can be inferred from the phase of ECA waveforms of individual subjects. The induced HFOs can, therefore, be utilized as a marker of successful re-calibration of the dysfunctional circuit generating PD symptoms.

Introduction

Chronic high-frequency (>100 Hz) deep brain stimulation (DBS) is an established medical treatment for movement disorders such as Parkinson's disease (PD) and is being explored for the treatment of many other neurological and psychiatric indications [1–3]. Yet, despite decades of clinical use, its underlying therapeutic mechanism is still unclear [1,2]. In particular, there is limited knowledge regarding the neural oscillatory modulations induced with therapeutic high frequency stimulation (HFS). If robust and target-specific neural signatures associated with HFS can be discovered, they can both assist to uncover the mechanism of DBS therapy and open the path for the construction of adaptive therapies which can tune the stimulation parameters for individual PD patients.

The studies seeking an electrophysiological basis for the mechanisms of DBS have focused on the investigation of neuronal spiking and oscillatory activity from the basal ganglia. Early hypotheses suggested that high-frequency DBS mimics lesioning by inhibiting neuronal firing from the stimulated structure [4–8]. Others proposed that DBS therapy overrides the pathological burst-type firings with its stimulus-induced regular (tonic) pattern and thereby ameliorated Parkinsonian symptoms [9–11]. This effect is not only in the stimulated structure but also travels downstream to the basal ganglia-thalamo-cortical circuit [10,12] and creates an "informational lesion" preventing the relay of pathological firing and oscillations [13]. However, other studies suggest that DBS, by regularizing basal ganglia spiking activity, enhances the information processing and restores responsiveness of the thalamocortical cells to the incoming sensorimotor information [14–16], indicating that rather than causing "lesioning", DBS might exert its therapeutic effect through promotion of neural activity similar to the "healthy" state [17,18].

Local field potentials (LFP) of the basal ganglia have long attracted interest due to their utility as a feedback modality for closed-loop DBS. Particularly in the subthalamic nucleus (STN), one of the frequently targeted structures in PD patients [19,20], excessive beta (12-30Hz) band oscillations are considered as the hallmark [21,22] and have shown to diminish with DBS [12,23,24] and dopaminergic medication [23,25,26]. More recently, the broadband high-frequency oscillations (200-450Hz, HFO) of LFPs and cross-frequency coupling between beta and HFO bands [27–30] have been identified as important markers in PD electrophysiology. Although the pharmaceutical modulations of the LFP bands (e.g., suppression of beta and enhancement in the HFO bands) have been well-documented [29–33], the large stimulus artifact observed during DBS have hindered further investigation of these biomarkers, especially in the HFO range, for closed-loop neuromodulation applications [34]. Consequently, the contribution of LFPs in uncovering the mechanisms of DBS have been limited due to the inability to record these oscillations during stimulation.

With these motivations, we established an intraoperative system to record LFPs during acute stimulation of STN in PD patients undergoing DBS surgery. We hypothesized that high-frequency stimulation (HFS) exerts its therapeutic effect by modulating oscillatory neural activity in the STN, similar to the effect of pharmaceutical treatment. To test this, we recorded LFPs intraoperatively from microelectrodes and studied their modulation out- and in-STN during multiple low- and high-frequency stimulation paradigms. We observed that high-frequency therapeutic DBS (>100Hz) induced HFO activity similar to the reports in the pharmacologically treated patients and healthy animals. In conjunction, we noted an evoked activity after each stimulus pulse, which was more resonant with the high-frequency stimulation. More interestingly, the strength of induced HFO was related to the interaction of stimulation pulses with the phase of evoked waveform, indicating that both measures and their characteristics can be used functionally to optimize electroceutical therapy.

Results

LFPs were recorded before, during and after stimulation in 16 STNs at various depths, from two bipolar microelectrodes separated by 2mm, as depicted in Figure 1A. Recordings were performed unilaterally from the STN contralateral to the most affected side in ten patients and bilaterally in three patients. The neural recordings started 15mm above the ventral border of STN (denoted as 0mm), and the "out-STN" stimulation was performed when the electrodes reached 10mm. The "in-STN" stimulation experiments were performed 2mm below the dorsal border of STN. The electrode with the most beta and HFO activity [35,36] was used for recording the LFPs from the stainless-steel rings situated 3 and 4mm above the tip, respectively. The LFP rings of the other electrode were used to deliver bipolar, biphasic, cathodic-leading stimulation at 2mA amplitude and 60us pulse width at various frequencies for 22 seconds. The recorded waveforms were checked for saturation visually and verified to be within the amplitude range of the recording amplifier (Figure 1B). The amplifier, with its high sampling frequency (38.4KHz) and large input range (±340mV), was able to capture the stimulation pulse without saturation and within a short duration (~250us, 9-10 samples), followed by evoked LFP activity.

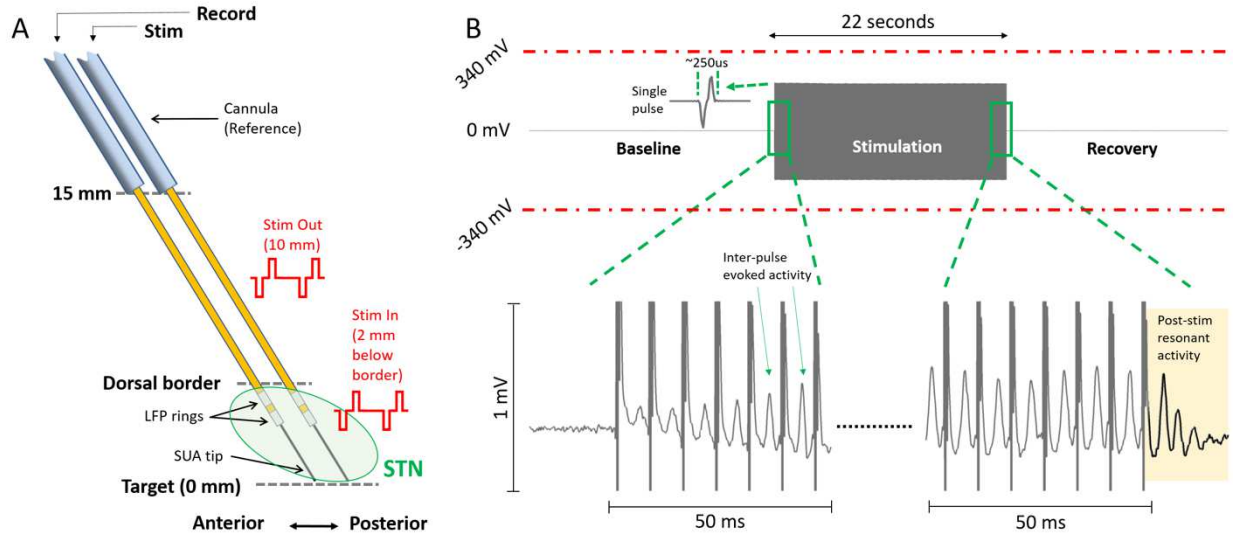

Figure 1: *Experimental paradigm and sample stimulation segment showing that LFP recordings did not saturate with the high input range of the amplifier. (A) The microelectrode diagrams depicting the recording and stimulating electrodes. The "out-STN" stimulation was performed 10mm above the ventral border of the STN. Bipolar microelectrodes with two 0.5mm wide stainless-steel rings separated by 0.5mm were used to deliver biphasic electrical stimulation and record LFP activity. The "in-STN" stimulation experiments were performed 2mm below the dorsal border of the STN, characterized by the increased background activity and neuronal spiking recorded from the fine microelectrode tip. (B) Sample 66s raw LFP recording illustrates that the amplifier was not saturated during stimulation of the other electrode. Single pulse waveform illustrates that the biphasic stimulation pulse was captured within a short time, allowing the LFP recordings to continue with minimal interruption. Zoomed 50ms segments from beginning and the end shows evoked potentials induced with each stimulus pulse. The evoked waveform amplitude increases with each pulse and settles after ~10 pulses. With the termination of the stimulation, the resonance in the evoked activity can be observed longer, which dampens within 20ms.*

High-frequency stimulation modulates HFO and evokes resonant compound activity in STN

The modulatory effects of therapeutic stimulation were explored with an "OUT vs. IN" STN stimulation paradigm to investigate whether there are STN-specific neural patterns. Figure 2A illustrates the changes in LFP spectrum before, during and after high-frequency stimulation (130 Hz), out- and in-STN for a representative subject. The left panels are the time-frequency maps (TFM) showing the temporal changes in the LFP spectrum, whereas the right panels represent the average spectral content of baseline and

stimulation periods of the corresponding TFMs. There was a consistent enhancement around 300 Hz induced by high-frequency stimulation in-STN, whereas no modulation was present out-STN with the same stimulation (Figure 2C, Wilcoxon signed-rank test, $p<0.001$, $n=10$). The modulated HFO disappeared immediately after the cessation of the stimulation. The lack of modulation out-STN suggests that the induced HFO activity is not a stimulation artifact.

The high-frequency stimulation also induced resonant evoked compound activity (ECA) in-STN between pulses (Figure 1B) as well as at the end of stimulation (Figure 2B, top). The amplitude of ECA, calculated as the amplitude difference between the first positive and the first negative peaks, was significantly higher in-STN (Figure 2D, Wilcoxon signed-rank test, $p<0.001$, $n=10$). Similarly, lack of observation of ECA out-STN suggests that this response is specific to STN and not a stimulation artifact (Figure 2B, bottom).

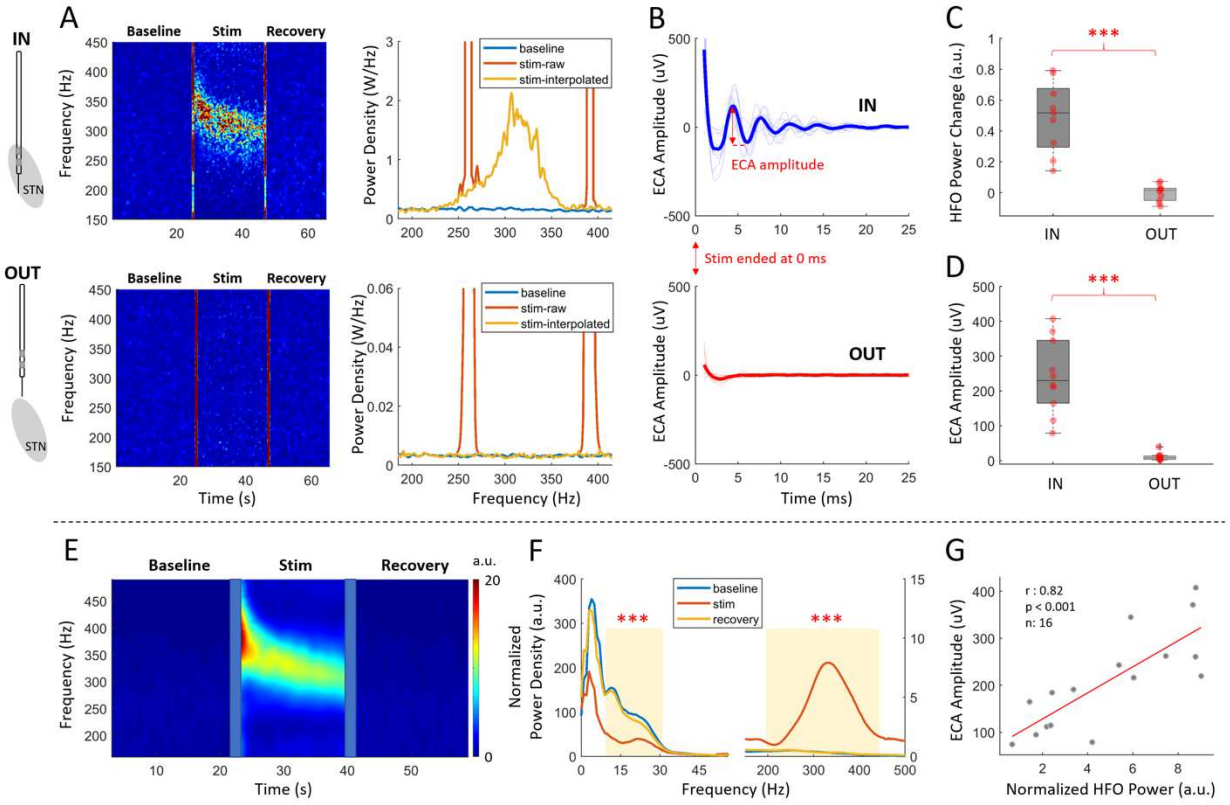

Figure 2: *HFO and resonant evoked compound activity are observed during high-frequency DBS only in the STN. In 10 hemispheres, 130Hz stimulation was performed out- and in-STN to identify and eliminate the artifacts caused by the stimulation or the recording hardware. (A) Representative TFM and PSD plots of out- and in-STN stimulation from a sample patient shows that HFO was induced only within the STN. The vertical red lines on TFMs are the transition artifacts associated with turning the stimulator on and off. The large artifacts caused by harmonics of the stimulation frequency are interpolated. The color scale of the TFMs are the same as the limits of the y-axis of their respective PSD plots. (B) The evoked response at the end of 22s stimulation was only seen in-STN. The thick lines illustrate the mean waveform. The first 1ms after the stimulation pulse is blanked out due to large artifact amplitude. (C) Comparison of the HFO power change between out- and in-STN stimulations show a significant difference (n=10). (D) Similarly, the difference between ECA amplitude of out- and in-STN stimulations was significant (n=10). (E) The grand average TFM from all 16 hemispheres with 130 Hz in-STN stimulation shows a stark enhancement in the HFO range, similar to the representative subject. The transition artifacts on TFM are masked with blue boxes. (F) The grand average PSD plots for baseline, stimulation and recovery periods from all 16 hemispheres with high-frequency stimulation in-STN. There was a significant suppression in the beta and significant enhancement in the HFO ranges (n=16). (G) In the STN, the ECA amplitude and induced HFO power correlated (n=16). *** denotes significance <0.001*

The average TFMs of all 16 hemispheres with 130 Hz stimulation in the STN is shown in Figure 2E. The enhancement of the HFO band in the group data was similar to that within the representative subject. As the corresponding average spectrum (Figure 2F) illustrates, there was a significant suppression in the beta band accompanied by a significant enhancement in the HFO range (Wilcoxon signed-rank test, $p<0.001$, $n=16$). The baseline and recovery sections had very similar spectral characteristics. The beta and HFO bandpowers or their change were not significantly correlated with each other. Interestingly, the enhanced HFO bandpower during stimulation was significantly correlated with ECA amplitude in the STN (Figure 2G, Spearman, $r=0.82$, $p<0.001$, $n=16$). Although beta band was also suppressed with stimulation, no significant correlation was found with ECA amplitude.

Low-frequency stimulation does not modulate HFO but induces non-resonant ECA in STN

To determine whether the HFO and ECA were specific indicators of therapeutic stimulation, we also delivered low-frequency 20 Hz stimulation in-STN. Figure 3A illustrates representative TFMs from before, during and after high- and low-frequency stimulation, respectively, in a representative patient. The modulation observed in the HFO range with 130 Hz stimulation was not present with 20 Hz stimulation. Similar to out-STN, group statistics revealed that there was no significant change in the HFO band during 20 Hz stimulation when compared to baseline. The power of the induced HFO activity was significantly different between 20Hz and 130Hz (Figure 3B, Wilcoxon signed-rank test, $p<0.001$, $n=13$).

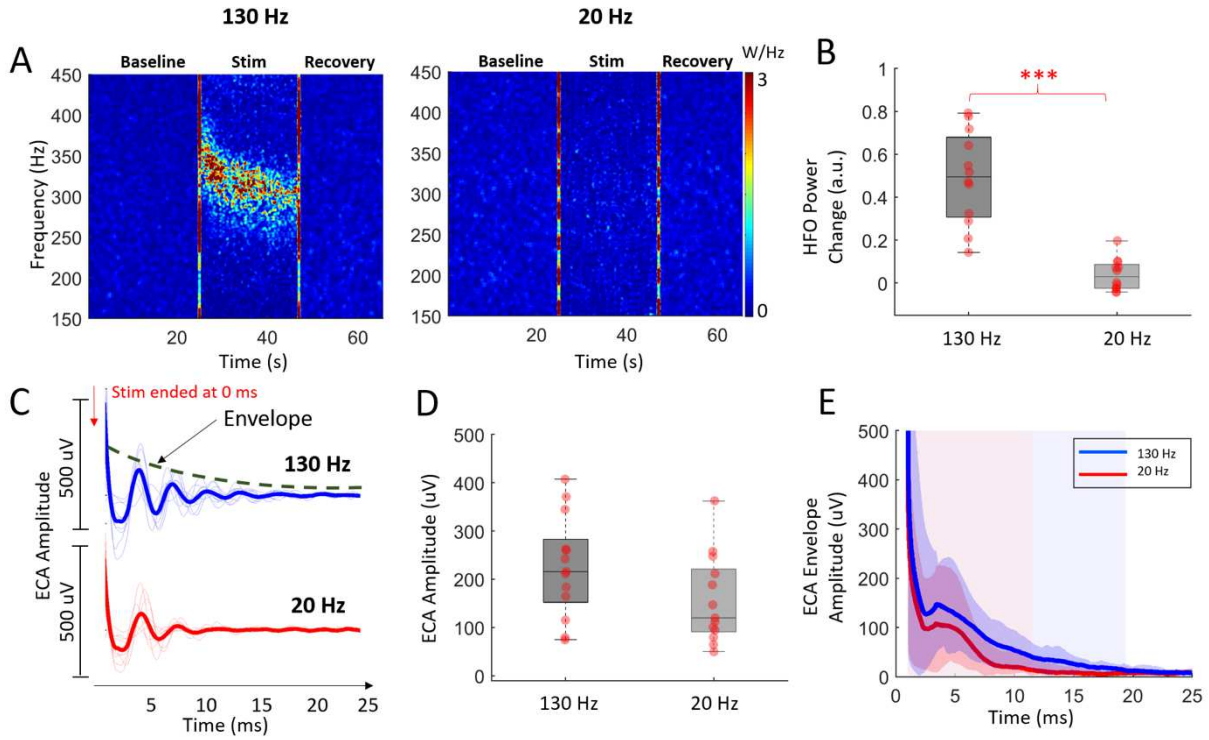

Figure 3: *Low-frequency DBS does not induce HFO but evokes compound activity that damped faster. (A) Representative TFMs of high- and low- frequency stimulation from a patient shows that HFO was induced only with the former. The large artifacts caused by harmonics of the stimulation frequency are interpolated. The vertical red lines on TFMs are the transition artifacts associated with turning the stimulator on and off. (B) The HFO power change was significantly higher with high-frequency stimulation (n=13). (C) Both high- and low- frequency stimulation induced ECA. The first 1ms after the stimulation pulse is omitted due to large artifact amplitude. (D) The difference between ECA amplitude after high- and low-frequency stimulation was only marginally significant (n=13). (E) The dampening of ECA derived from the envelope of the Hilbert transform of the waveforms was significantly faster after low-frequency stimulation (19ms vs 11ms, n=13). *** denotes significance <0.001.*

Despite the lack of modulation in the LFP spectrum in the HFO range, interestingly, the ECA was still present with low-frequency stimulation (Figure 3C). The amplitude of the 20 Hz ECA was slightly smaller than that of the 130 Hz, however the difference was not significant (Figure 3D, Wilcoxon signed-rank test, p=0.057, n=13) and the activity was no longer as resonant as 130Hz stimulation and damped earlier, as illustrated in Figure 3C and E (19ms vs 11ms, one tailed t-test, p<0.05, n=13).

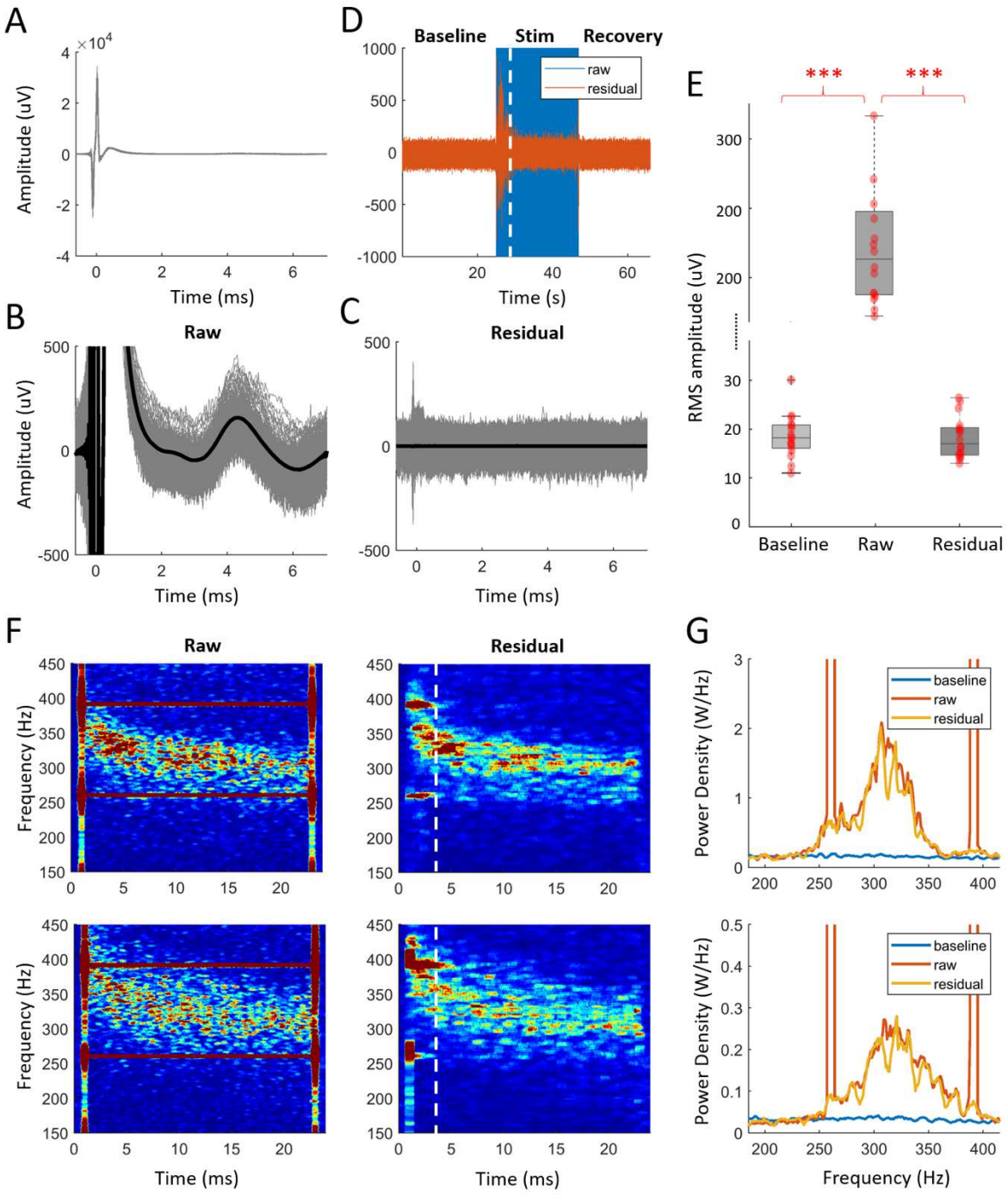

Figure 4: *HFO induced by therapeutic 130 Hz DBS is present even after removal of evoked waveform between stimulation pulses. (A) The overlay plot of raw data aligned with respect to the stimulus pulses (0.5ms pre-onset was used to avoid edge artifacts). The large biphasic stimulation artifact at 0ms masks both ECA and other LFP activity. (B, C) The same segment in A shown with*

*1mV amplitude scale before and after denoising, to better demonstrate the removal of ECA waveform between pulses (thicker lines indicate the average waveform). The residual was obtained by subtraction of reconstructed segments from the raw data and it is devoid of stimulus pulse and inter-pulse evoked activity. (D) The amplitude range of the denoised (residual) data is similar to the baseline levels, except the first 3s seconds of transient period. This segment, denoted with the dashed lines, was removed from overlay plots for clarity and excluded from bandpower calculations as well. (E) The root-mean-square (RMS) amplitude of the baseline segment before stimulation as well as raw and residual traces during stimulation. There was no significant difference between baseline and the denoised stimulation segment (n=16). The first 1ms including the large stimulation artifact was omitted from the RMS calculations to capture the amplitude levels associated with the evoked response. (F) TFM of the raw and residual segments and (G) their PSD plots from two representative patients illustrate that the denoising primarily removes the artifacts at the harmonics of stimulation frequency while keeping the enhanced HFO intact. The color scale of the TFMs are same as limits of y-axis of their corresponding PSD plots. The dashed lines on TFMs denote the transition artifacts associated with turning the stimulator on and off. *** denotes significance <0.001*

HFO power is independent from ECA observed between stimulation pulses

The correlation observed between induced HFO bandpower and the amplitude of evoked resonant compound activity with HFS was relatively high (Figure 2G, r=0.82, p<0.001). Naturally, the HFO could be an epiphenomenon of the ECA between stimulation pulse. To test whether these two phenomena are dependent, we executed an adaptive denoising process to remove the inter-pulse ECA as well as the large amplitude stimulation artifacts from the LFP data. A moving average template removal filter (see Methods section for the details) was applied to the raw data, in order to isolate and remove the evoked peaks during stimulation. Figure 4A illustrates the representative raw LFP data segmented around the stimulation pulses. The large biphasic stimulation pulse artifact at 0s is much larger in amplitude in comparison to ECA and typical LFP oscillations. Figure 4B shows the same segments with 1mV amplitude range, revealing the ECA waveforms between stimulation pulses (Figure 1B). The templates of ECA waveform following each stimulation pulse as well as the stimulation artifact is reconstructed from these segments. The residual data (reconstructed signal subtracted from raw signal, Figure 4C) was considered as denoised LFP. The denoising process removed the large stimulation artifact as well as the ECA observed between pulses. Figure 4D demonstrates that the denoising achieved amplitude ranges comparable to the baseline segment before and after the stimulation, except the short 3s transient period in the beginning which was excluded from further analysis. Figure 4E compares the root-mean-square (RMS) amplitude of baseline segment with that of raw and residual segments in all hemispheres. While baseline and residual segments were not statistically different, the raw stimulation segment was significantly larger in amplitude (Wilcoxon signed-rank test, p<0.001, n=16). The first 1ms which involves the large stimulation artifact (Figure 4A) was removed from the RMS amplitude calculations to prevent the masking of evoked activity by the stimulation artifact. Figure 4F and G show the TFMs and the corresponding spectra from two representative subjects during stimulation. The denoising process suppressed the large spectral artifacts at the harmonics of stimulation frequency. Although the ECA has been removed from the raw data (Figure 4C), it did not change the spectral content of the LFP in the HFO range as much and the correlation between ECA amplitude and HFO power from the denoised traces remained the same (Spearman, r=0.82, p<0.001, n=16), suggesting that HFS induced ECA and HFO are independent.

Frequency dependent modulation of ECA and HFO activity

The dependency of ECA and HFO activity on the stimulation frequency was tested by stimulation of STN with 130, 160 and 180 Hz. Figure 5A shows that the enhancement in the HFO band was visible during all 130, 160 and 180 Hz DBS in a representative subject. The representative evoked waveforms at the end of stimulation in Figure 5B also show that all three stimulations induced resonance in ECA. We further investigated population response of these metrics. Figure 5C illustrates that the ECA amplitude was significantly smaller with 180 Hz stimulation when compared to the others (Wilcoxon signed-rank test, p<0.01, n=9), which were not significantly different. Although all high-frequencies induced HFOs, a

downward trend was observed in HFO power with increased stimulation frequency but the differences among groups was only significant between 130 and 180 Hz (Figure 5D, p=0.04). The level of beta suppression was not significantly different between groups. Similar to Figure 2E, the center frequency of HFO was higher residing between 350-450Hz range during the initial phase of the stimulation and later it decreased, settling around 300-350Hz (Figure S1). However, there was no difference between groups in terms of peak frequency in the first and the last two seconds of stimulation (Figure 5E, Wilcoxon signed-rank test, p<0.01, n=9). Finally, we correlated the HFO enhancement with ECA amplitude for patients with multi-frequency therapeutic stimulation. There was still a significant correlation of 0.77 (Spearman, p<0.01, n=27) between ECA amplitude and HFO bandpower induced by all high-frequency stimulations.

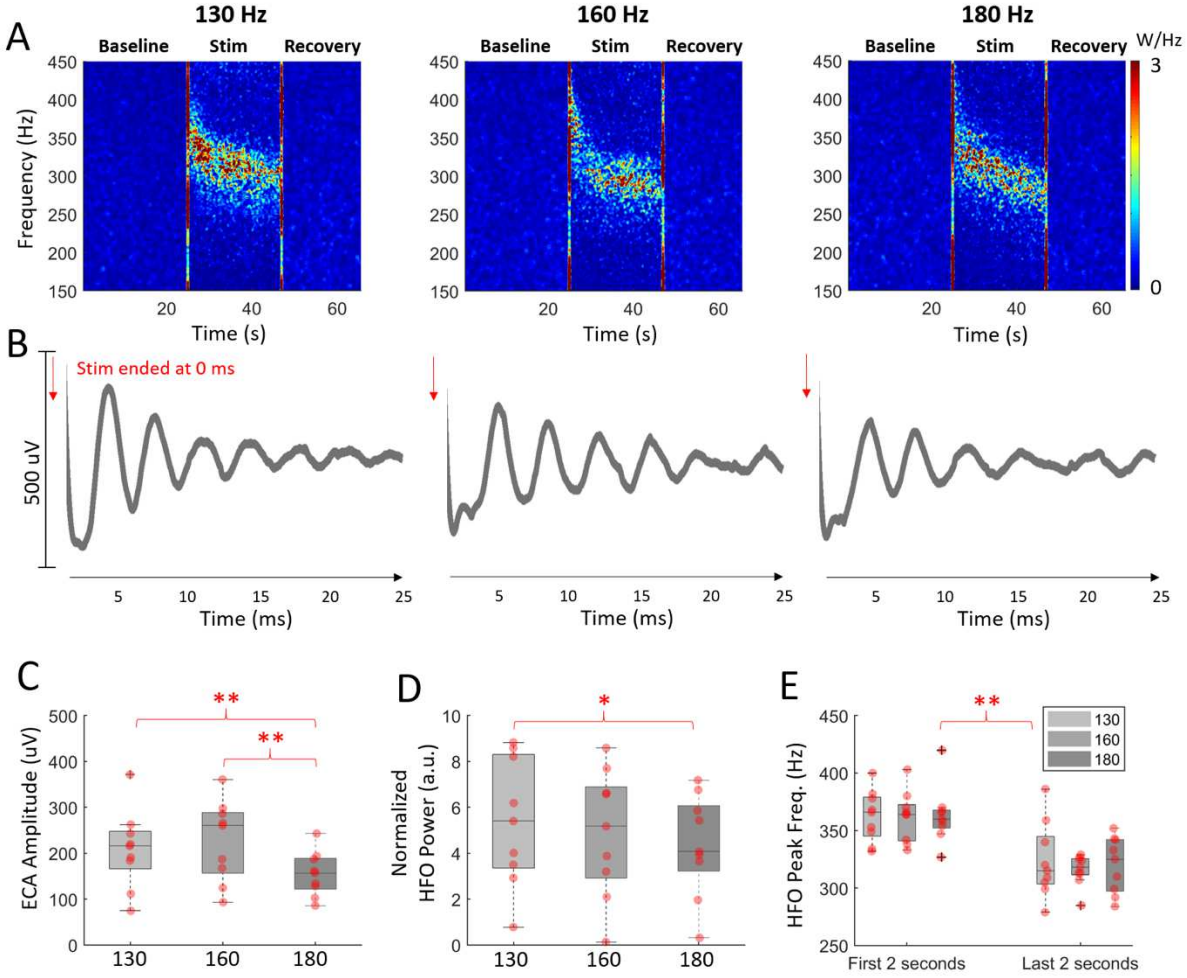

Figure 5: *High-frequency stimulations modulate HFO and ECA in different amplitudes. (A) The HFO was enhanced with all stimulation frequencies. The large artifacts caused by harmonics of the stimulation frequency are interpolated. The vertical red lines on TFMs are the transition artifacts associated with turning the stimulator on and off. (B) The ECA waveform after 22s stimulation period was resonant after all high-frequency stimulations. The first 1ms after the stimulation pulse is omitted due to large artifact amplitude. (C) The comparison ECA amplitude after 22s of stimulation showed that ECA after 180 Hz stimulation was significantly smaller (n=9). (D) The induced HFO bandpowers were only significantly different between 130 and 180 Hz groups (n=9). (E) The peak frequency of HFO in the first and last two seconds of stimulation were significantly different in all groups (n=9) but not different between groups. ** denotes significance <0.01, * denotes significance <0.05*

Despite lack of difference in HFO peak frequency during 130, 160, 180 Hz stimulation and ECA morphology after it, the inter-pulse evoked waveforms varied between these groups. Figure 6A illustrates aligned inter-pulse evoked activity over 22s of stimulation with various frequencies in a representative patient. While high-frequency stimulation caused an adaptation in the timing of first evoked peak, this was not observed in low-frequency stimulation. Figure 6B quantifies the adaptation by comparing the delay of the first peak after stimulus pulse at the time periods of 0-2, 8-10 and post-stimulation. 8-10s point was selected since after 10s, ECA peak in 180 Hz was out of range. As illustrated in the representative subject as well, 130 Hz stimulation settled very quickly compared to 160 and 180 Hz stimulation (the difference between post-stim ECA delay was still significant after 8-10s, Wilcoxon signed-rank test, $p<0.01$ for 160Hz and $p=0.04$ for 180Hz, $n=9$). With 20 Hz stimulation, the ECA delay between pulses was stable throughout the stimulation period.

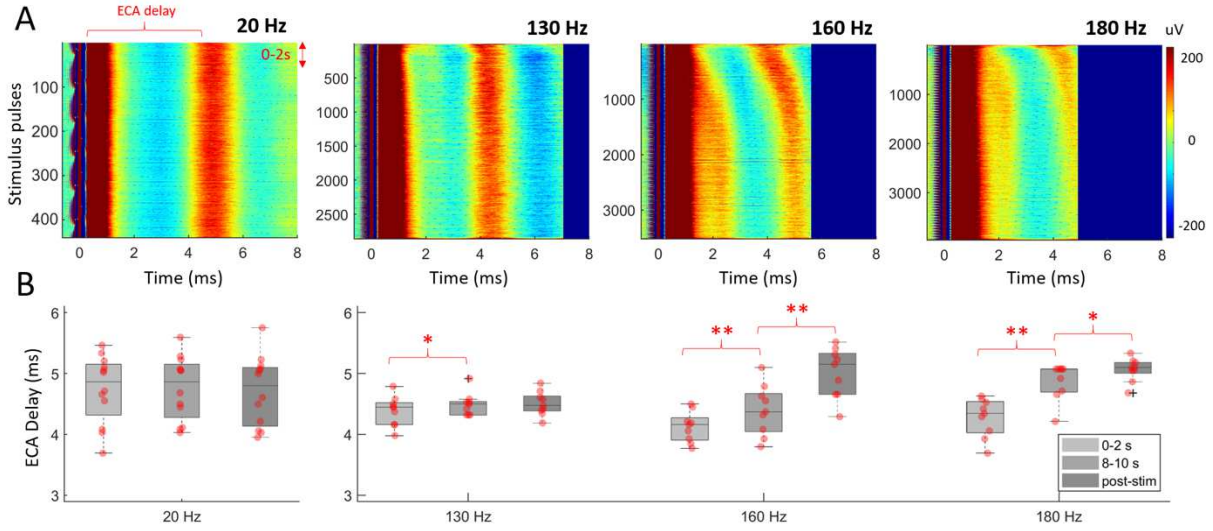

Figure 6: *Inter-pulse evoked activity shows adaptation only with high-frequency stimulation. (A) The representative aligned raw data with respect to the stimulus pulse for 130, 160, 180 and 20 Hz stimulation (0.5ms pre-onset, up to 8ms is shown). (B) The ECA delay comparison in the 0-2s, 8-10s and after 22s demonstrate the differences in adaptation between 130, 160, 180 (n=9) and 20 Hz (n=13) stimulations. The ECA delay, which denotes the delay of the first evoked peak, was consistent throughout the 20 Hz stimulation period, indicating no adaptation. The fastest adaptation was with 130 Hz, settling after 2s. ** denotes significance <0.01, * denotes significance <0.05.*

HFO power favors specific phases of ECA waveform

In an effort to explain why HFO was modulated differently with 130, 160, 180 Hz stimulation, we investigated whether the timing of stimulation pulse and the ECA phase affects the modulated HFO power. We utilized the phase of ECA waveform during 20 Hz stimulation, due to its stationary behavior. The consistent delay throughout the 20 Hz stimulation period, as seen in Figure 6, assures that the ECA is not enforced to adaptation. The high sampling frequency of the recording amplifier allowing for a more accurate estimation of the phase, which could have been problematic with conventional sampling rates for LFPs (~2 KHz). Figure 7A shows the ECA waveforms after 22s of low-frequency stimulation from six patients who had a 20 Hz stimulation experiment in addition to 130, 160 and 180 Hz. The location of the red circles denotes where each 130, 160 and 180 Hz stimulation pulse would appear if they were the stimulation frequency. The size of the circle corresponds to the relative HFO bandpower that stimulation induced in each patient. The instantaneous phase information is extracted using Hilbert transform, and

represented with arrow with a length corresponding to the relative strength of the induced HFO activity (Figure 7B). The circular one sample test for mean angle [37] show that the preferred phase was between 143-275 degrees (circ_mtest, p<0.01, n=6). This behavior could be likened to a pendulum or a children's swing, where the push needs to be made at the right time or phase for the increased effect (Figure 7C).

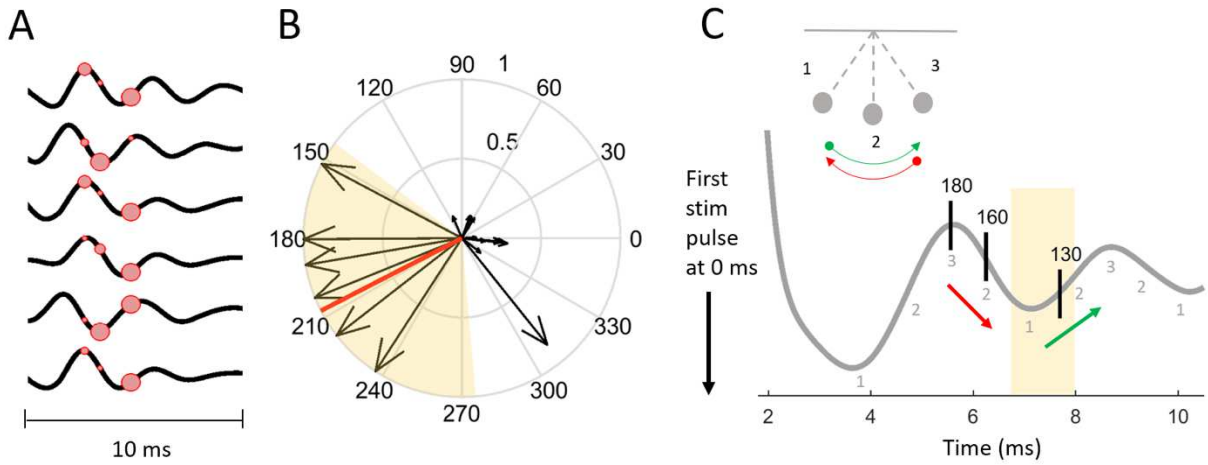

***Figure 7**: The DBS can be tuned to provide maximum modulatory effect based on the phase of ECA waveform. (A) The ECA waveforms after 22s of low-frequency stimulation from the six subjects with both 20 Hz and high-frequency stimulation experiments. The location of the red circles denotes where the next 130, 160 and 180 Hz stimulation pulses would be, if the stimulation continued with the specified frequency. The size of the circle denotes the relative amplitude of the induced HFO by that stimulation. (B) The information in A is presented on polar coordinates to illustrate the phase preference. The arrow length denotes the relative amplitude of the induced HFO power. The mean angle was 208 degrees and is denoted by the red line. The preferred phase was between 143-275 degrees (n=6) and is denoted by the highlighted background. (C) A pendulum and a representative ECA waveform to illustrate the swing-like behavior of the evoked response. The numbers indicate the positions of pendulum. The shaded region illustrates the preferred phase angles from B. When the next stimulation pulse is at a preferred phase location (forward motion, green), the modulatory effects can be enhanced. On the other hand, stimulating at the other phase (backward motion, red) could hinder effect of DBS.*

Discussion

To investigate the mechanisms of electroceutical therapy in PD, we have studied the oscillatory neural dynamics of STN-LFPs intraoperatively during low and high-frequency stimulation. We observed that high-frequency stimulation at >100Hz induced HFOs in 300-450Hz range as well as an independent evoked resonant compound activity. When DBS was delivered at a non-therapeutic low-frequency at 20Hz, the HFO did not modulate and the evoked compound activity was not as resonant. We also observed that despite having similar modulations, HFO power varies with the therapeutic DBS at different frequencies (130, 160 and 180Hz), depending on the ECA phase. Our findings suggest that DBS may exert its therapeutic effect by bringing neuronal populations to a "healthy" or "treated" oscillatory state, and the stimulation frequency to maximize these oscillations can be inferred from ECA waveforms.

Modulated HFO Is not an Artifact and Is Independent of ECA

The relatively high stimulation voltage (V range) and subsequent artifact in the recording systems have historically prevented the exploration of LFPs (uV range), especially in the HFO band due to overlapping artifact harmonics. Therefore, in addition to recording LFPs with an amplifier with large input amplitude range (±340mV) and relatively high sampling frequency (38.4kHz), we performed the stimulation

experiments in- and out-STN to establish that observed neural modulations are not due to stimulus or saturation artifacts (Figure 1A). We also ensured that the assessed waveforms during stimulation were within the dynamic recording range of our amplifier (Figure 1B), which is crucial for the reliability of observed patterns. While HFO was induced only with high-frequency therapeutic DBS (Figure 2A, C, E, F), evoked activity was present with both therapeutic and non-therapeutic DBS (Figure 3C, D) only during in-STN stimulation. There was neither evoked response during out-STN stimulation experiments nor HFO was induced (Figure 2A-D), indicating that both HFO and evoked activity are physiological responses, not mere artifacts.

There was a high correlation between ECA amplitude and HFO power (r=0.82, Figure 2G), which implied that one could be an epiphenomenon of the other. Later, the dependence of HFO and evoked resonant activity was tested following a denoising process. Specifically, after employing a temporal template extraction filter, we reconstructed the DBS artifact at each pulse and the associated evoked response between pulses, devoid of any LFP activity. This reconstruction was then subtracted from the raw signal to obtain the denoised (residual) data (Figure 4C). When the spectral content of the raw and residual data was compared (Figure 4F, G), we observed almost no change in the HFO power. Even though both the DBS pulse artifacts and the evoked waveform were substantially eliminated, the high correlation between ECA amplitude and HFO power was sustained. Furthermore, although we observed an ECA with 20 Hz stimulation at similar amplitude levels (Figure 6A), there was no simultaneous HFO enhancement (Figure 3A, Figure S2). Consequently, the existence of HFO activity with HFS even after the removal of the evoked response and observation of evoked activity without HFO during low frequency stimulation suggest that HFO modulation is independent of ECA and not an epiphenomenon.

Resonant versus non-resonant evoked activity

Evoked compound activity has been reported in various structures of the nervous system, such as hippocampus [38], spinal cord [39,40], cortex [41] as well as the STN of PD patients [42–44]. Specifically, it was observed that STN-DBS causes evoked response in other structures such as cortex [45,46] and both internal and external parts of globus pallidus [47]. In PD-STN, it was shown that the ECA during therapeutic DBS can be used to identify clinically beneficial amplitudes [42]. Using a custom stimulation scheme, Sinclair et al. [43] recently has demonstrated that evoked resonant activity can also be used to locate the most beneficial stimulation site. We also observed ECA during high-frequency DBS (Figure 2B). Additionally, we studied stimulation at different frequencies and found that the evoked response exists in the STN with 20, 130, 160 and 180 Hz (Figure 3C, Figure 5B). While both high- and low-frequency stimulation produced similarly strong ECA (Figure 3D), the response was significantly more resonant with HFS and lasted longer after cessation of DBS (19 versus 11 ms, Figure 3E).

The ECA induced with various stimulation frequencies can be due to the propagation of activity to other structures through projections forming loops [48]. Previously, a stereotypical periodic pattern of neuronal responses in globus pallidus (both interna and externa), putamen, and cortex were reported that were same at low (50 Hz) and high frequency (100 and 130 Hz) STN-DBS immediately consequent to the DBS pulse [48]. This periodic form of activity has returned to the baseline after ~8ms not only in these structures but also in STN [6]. Since STN sits in a highly interconnected cortico-basal ganglia-thalamo-cortical network, stimulus at high-frequency might have induced ECA in an underdamped oscillatory form through the feedback loops [1,49,50]. Additionally, given that ECA can even be recorded from the spinal cord [39,40], it is likely that the ECA represents the response of a larger network and not necessarily a local circuit.

The reason for the longer lasting resonance with high-frequency stimulation can be explained with a pendulum/swing analogy (Figure 7C). If each stimulus pulse is the force pushing the pendulum (i.e., the network) in one direction, with low-frequency stimulation, there is a longer period between each push (i.e. stimulus pulse) and that this duration is long enough for the pendulum to reach equilibrium. Therefore, we observe a steady response in ECA morphology over 22s of stimulation for 20Hz (Figure 6) as the response completely dampens before the next pulse hits the system. However, with frequent hits not allowing the pendulum to come to a stop, high-frequency stimulation starts to activate a larger pool of neurons or a network yielding resonance by injecting sufficient paced energy to the system. Our observations provide electrophysiological evidence for the "Resonance and Carrier Signal Effect" hypothesis of Montgomery and colleagues [48,51,52], which proposes that the resonant ECA is the form of amplified periodic responses to the consecutive stimulation pulses, in accordance with the definition of resonance is physics.

The adaptation on the inter-pulse evoked response (Figure 6) shows that the network reaches a steady state after an initial ramp-up period (3-10s) with stimulation at high-frequencies and in particular a longer delay at 160 and 180Hz (Figure 6B). In that sense, therapeutic DBS likely entrains the network [53] to its steady state over several seconds based on the consistence of the response from the intrinsic oscillators in the system to the first and consecutive future pulses [51,54]. While there are likely multiple oscillators within the basal ganglia-thalamo-cortical system, it has been suggested that the main or average frequency is approximately 130Hz [48,51].

It is also possible that resonance in ECA is due to total injected energy, similar to a large push to the pendulum causing a longer lasting swing. In that case, even 20Hz stimulation with high amplitude might cause a longer lasting evoked response. However, an animal study reported that even at high amplitudes, 20Hz stimulation did not pace the subthalamic neurons, as it did during >100Hz stimulation [55]. The same group also reported that the pulses must be close enough to one another to override the deleterious STN activity [56].

Modulation of the multiscale neural activity with dopaminergic medication and therapeutic DBS

We observed HFO activity initially starting at 350-400Hz range and later settling around 300Hz during high frequency stimulation of STN (Figure 2E, Figure 5A, E, Figure S1). There is an abundance of reports regarding the modulation of ~300Hz HFO in the STN of PD patients undergoing dopaminergic therapy [29–33]. The HFO activity appears concurrently with the therapeutic effect of the medication, representing the "ON state" [29,31,32]. This rhythm was suggested to be a "coordinating clock" that paces the neural excitability [31]. Indeed, it has been proposed that the bidirectional connection between STN and the external segment of the globus pallidus is well-positioned to form a "central pacemaker" in the basal ganglia [57–59]. The physiological ~3ms synaptic transmission delay between these two structures [10,60] could explain the genesis of ~300Hz HFOs as an indication of functioning pacemaker. Although there are no reports of LFP activity in the healthy human STN, similar HFO activity centered around 300Hz has been observed in the healthy non-human primates and disappeared after 1-methyl-4-phenyl-1,2,3,6-tetrahydropyridine (MPTP) treatment inducing PD (see Figure 1 in Escobar et al., 2017). The lack of 300Hz HFO activity or deviation from it in STN could be a marker of disease state, and high-frequency DBS might be restoring the HFOs to their healthy state similar to pharmacological treatment. There is further evidence that nonlinear features extracted from HFOs correlated with improvements of motor function in patients with PD proposing that HFOs might contain vital information about the disease state or its severity [29–33].

At a finer scale, earlier studies on non-human primates reported an increase in bursting neuronal activity and instantaneous firing rates after MPTP treatment [62,63] suggesting that the emergence of bursting firing is a marker of PD state. Later, STN DBS at 130 Hz has been reported to restore motor function in MPTP-treated primates and 6-hydroxydopamine (6-OHDA) treated rats by inducing more regular firing patterns, higher average firing rates, and lower burstiness [6,10,48,64,65]. These observations in the form of the migration from bursting to regular firing due to high-frequency DBS were further confirmed with a computational model of the cortico-basal ganglia-thalamo-cortical loop in both normal and parkinsonian conditions [18]. Since single neuronal recordings are not common in PD patients in the medicated state, not much was known regarding the neuronal firing patterns in STN modulated with dopaminergic therapy. Our recent case report investigating the firing patterns of individual neurons and HFO activity in STN intraoperatively has provided a unique opportunity to observe the multiscale neural activity in a PD patient after dopaminergic treatment state [66]. We reported that the STN was dominated with 300Hz HFO activity and there were no pathological burst-type firings in the medicated state. In this subject, unlike recordings from PD patients in the unmedicated state [67,68], tonic (regular) spiking was observed together with ~300Hz HFOs instead of bursts-type firings, with results matching the experimental observation of the regularizing effects of therapeutic STN-DBS on firing rates of STN [11,55] and other basal ganglia structures [9,10,53,69]. Although it was a single case, the ~300Hz HFO and regular/tonic neuronal firings in STN with dopaminergic medication [66] resemble to the regular spiking activity reported previously [9–11] and the 300-400Hz oscillatory response presented here during high-frequency DBS, suggesting that the mechanisms of both therapies might be similar as well. It was proposed that DBS therapy overrides the pathological burst-type firings with a stimulus induced regular (tonic) pattern [9]. Interestingly, earlier computational simulations on information processing through neuronal circuits also suggested that low-frequency and irregular spiking activity has an impairing effect on information processing while high-frequency and regular activity is the least deleterious [16,70].

It is important to note that a contradictory hypothesis was suggested by Sinclair et al. [44], since the authors report a decrease in HFO frequency after high- frequency DBS. The authors suggested that DBS and dopaminergic therapy have different mechanisms of action. For the reasons including saturation and large stimulus artifact, past work generally focused on the LFP activity in the lower frequencies during stimulation [9,24] or following the cessation of stimulation [44,71] with the presumption that neuronal activity observed immediately after stimulation would be representative of neuronal activity during stimulation. However, it has been shown that, after the application of artifact removal algorithms, what happens after stimulation does not necessarily reflect the changes in the neural activity during DBS [72]. In 16 STNs recorded, we observed a consistent power enhancement in the HFO range around 300Hz (Figure 2E, F) during stimulation, indicating that the high-frequency therapeutic DBS may have similar mechanisms to pharmaceutical therapy [73], which is to drive the basal ganglia circuit into a physiological oscillatory equilibrium [17,31]. Consequently, DBS may function by promoting neural activity similar to the stable electrophysiological state in the basal ganglia [55].

Electrophysiological basis for selection of optimal DBS frequency

Clinical observations suggest that high frequency stimulation (>100Hz) of STN and pallidum is therapeutic for Parkinson's disease [52,74,75], whereas low frequency DBS has does not affect or worsens symptoms [76,77]. The current understanding of mechanism of DBS is that high-frequency DBS saturates the neuronal response (driving neurons into the refractory period) and creates informational lesions [13,78]. In that case, the higher stimulation frequencies should have resulted in better therapeutic response, due to faster

repetition as well as the more energy delivered when applied with same amplitude and pulse width. Yet, the studies exploring the frequency as a parameter for DBS have reported that although >100Hz stimulation can ameliorate the effects of PD [74,75,79], ~130 Hz produced the most corrective response. They report, as the stimulation frequency increases further away from 130 Hz, especially after 160 Hz, the clinical benefits starts to decrease [48,75,79]. These experimental observations were further validated with a computational model of the cortico-basal ganglia-thalamo-cortical loop in both normal and parkinsonian conditions [18]. When contrasting various high-frequency stimulations at 130, 160 and 180Hz, we observed that the power of induced HFO and ECA amplitude were different (Figure 5C, D). Specifically, 180 Hz has consistently provided the lowest HFO enhancement and resonant ECA generation. Therefore, the amplitude of ECA waveform and power of HFO band can potentially be used as biomarkers to assess the therapeutic efficacy of DBS.

Although we show the HFO modulations are generally stronger with 130 Hz, this may not be the case in an individual patient. Then, how can one find the most therapeutic frequency for a specific patient? We found that there was a relationship between HFO strength and the instantaneous phase at which each pulse hit the ECA waveform (Figure 7). Specifically, we noted that a certain portion of the ECA phase space promoted the HFO. The highlighted phase intervals are likely the positions of consecutive stimulation pulses promoting resonance. Overall, these observations indicate that although there is a wide range of frequencies that can be used for HFS, it is likely that only a limited range will be effective in promoting maximum resonance yielding better therapeutic outcomes for an individual subject, depending on their intrinsic physiological oscillatory state. These observations are in line with the previous work involving computational simulations [18] and human subjects [75,79]. Going back to our analogy in Figure 7C, the ECA phase might correspond to different positions of the pendulum. Thus, although DBS at multiple high-frequencies might provide some level of clinical benefit for a patient as shown by previous studies, one could pinpoint the most efficient one by checking the ECA waveform and the power of modulated HFO band. In such a system, one could stimulate the patient with non-therapeutic low-frequency for a short time and propose a range for the optimal DBS frequency based on the temporal characteristics of the resulting ECA waveform. Current closed-loop DBS paradigms only focus on the amplitude of the stimulation. Yet, the adaptation of all parameters is needed for a truly adaptive DBS therapy. Here we presented the frequency optimization, but future studies will be conducted to test whether the induced HFO can be utilized to optimize the other parameters.

Burden on the beta band

Suppression of exaggerated beta band oscillations in the STN of PD patients with DBS [9,24,80] and dopaminergic therapy [25,29,31,32,81] is a well-established phenomenon. We also observed a significant decrease in beta power with high-frequency stimulation as well but there was no correlation with evoked activity amplitude. A compelling argument for the lack of such a relationship could be that the beta band is associated with many healthy functions in the brain, such as its suppression with movement or even planning or imagination of it [82,83], its modulations with wakefulness [84,85] and decision-making [86]. Therefore, despite established reports of its modulations in PD, the multifaceted involvement of beta band in physiological processes might make it a poor biomarker by itself for the diseased state, especially in the freely behaving patients with a chronic DBS implant. It is likely that, as Foffani et al. [31] proposed, there might be a high-frequency “clock” that is not directly involved in motor functions, but rather regulating the neural synchrony in order to guarantee the specific modulation of individual actions that are controlled by lower frequencies. Therefore, we speculate that beta band must be -at least- combined with

other state specific biomarkers for robust and reliable operation of long-term adaptive stimulation schemes such as closed-loop chronic DBS.

Conclusion

In this work, we have presented unique electrophysiological modulations in the STN with therapeutic DBS that shed light onto the mechanisms of the electroceutical therapy in PD. We observed that at high-frequencies, stimulation induces HFOs similar to what is reported in healthy primates and PD patients under dopaminergic treatment. More importantly, we observed that the stimulation frequency maximizing these oscillations in individual subjects could be inferred by the phase of ECA waveform, opening the doors for a truly adaptive DBS where not only the amplitude but the frequency of stimulation is also optimized for individuals. Future studies with more subject are warranted regarding the use of ECA phase – HFO power relationship in closed-loop therapy as well as the establishment of these patterns in other brain structures and disorders.

Methods

Patients

Thirteen patients (two females) with PD undergoing awake bilateral STN-DBS implantation at Baylor St. Luke's Medical Center were included in the study. Their ages ranged from 53 to 70 (mean ± standard deviation = 60.5±4.7). Recordings from three patients were obtained bilaterally and the rest of the patients were recorded unilaterally from the hemisphere contralateral to the most affected side. The types of experiments performed in each patient are denoted in Table S1. Briefly, the "in vs out STN stimulation" paradigm was executed in ten hemispheres and was stopped since the statistical significance was achieved. "Multiple high-frequency stimulation" paradigm was executed beginning with patient 5. Stimulations with 130, 160 and 180 Hz were delivered in a randomized order. However, 20Hz stimulation was not performed due to time constraints in patients 8-10. Similarly, we stopped recruiting subjects once the results were statistically significant. The study protocol was approved by the Institutional Review Boards of Baylor College of Medicine and University of Houston. All patients provided written informed consent.

Surgery and Recordings

Patients were requested to stop medication at least 12 hours prior to the surgery and all recordings were obtained in the awake state using local anesthesia. The stereotactic coordinates and trajectories to the STN were identified by fusing preoperative magnetic resonance imaging (MRI) and computerized tomography (CT) scans on a neuro-navigational platform (StealthStation S7, Medtronic, Ireland). In each hemisphere, awake recordings were performed to validate the targeting, using a set of two parallel microelectrodes separated by 2 mm (center-to-center) using the 5-cannula BenGun with "+" configuration. Additional to the center track, one of the anterior, posterior, lateral or medial tracks was selected by the neurosurgeon on a patient specific basis through analysis of the preoperative MRI. The bipolar microelectrodes (Microprobes for Life Sciences Inc, MD, USA, Figure S3) were initially placed at 15mm above the ventral border of the STN and advanced towards the target in 0.5-1mm steps using NeuroOmega drive (AlphaOmega, Israel) (Figure 1). The dorsal border of STN was determined in real-time by an experienced neurologist via visual and auditory inspection of the single unit firings from the high-impedance tungsten tip (0.4-0.8 MOhm), per standard clinical protocol. The dorsal STN border was

identified with a prominent increase in the background activity and spiking. The LFPs were recorded from the 0.5mm wide stainless-steel rings (3 and 3.5mm above the tip, 3-4KOhm impedance) located on the shaft of the electrode. The cannula was used as reference. The stimulation experiments were performed at 10mm above (Out-STN) and 2mm below (In-STN) the dorsal border, (Figure 1). The recordings were obtained with the gHiamp bio-amplifier (gTec, Austria) at 38.4 KHz sampling frequency, 24bit A/D resolution and ±340 mV input range. The biphasic stimulation with 60us pulse width and 2mA amplitude was delivered bipolarly from one of the microelectrodes using the Grapevine neural processor (Ripple, UT, USA). The data was stored in a computer hard drive for offline processing.

Signal Processing

The data acquisition, stimulation and processing were performed using custom developed scripts in Matlab R2014a (Mathworks, MA). The raw LFP traces were visualized to ensure the recordings were within the input range of the amplifier (±340 mV). The traces were forward and backward filtered with a 2nd order Butterworth high-pass filter with 2Hz cut-off frequency. The spectral analyses were conducted using Thompson multi-taper estimate with 4 slepian windows for each 1s of data (with 50% overlap). The large artifacts caused by harmonics of the stimulation frequency were interpolated with 5 Hz width for high-frequency stimulation and with 1.5 Hz width for low-frequency stimulation. The spectra were normalized using the mean activity between 500-600 Hz to account for amplitude differences between patients and smoothed with Matlab's "smoothdata" ("rloess" method was used) for frequencies over 100 Hz. From the spectrogram, the beta and HFO bandpowers were calculated as mean power between 12-30Hz and 200-450Hz respectively.

Evoked activity waveforms were processed by subtraction of a fitted exponential first, to remove the decaying response from the amplifier settling. The waveform was then smoothed with a Savitzky-Golay filter [87]. The processing did not affect the morphology or the duration of the evoked activity. The evoked waveforms were analyzed monopolarly, since the waveform was present on both contacts. To quantify the resonance, the envelope of the ECA was detected using Hilbert transform, and the first 20 ms of the envelope at every point was compared to the mean envelope between 20-25ms after stimulation to check for significant difference (one tailed t-test, $p<0.05$).

Inter-pulse evoked activity was reconstructed from the segmented traces, in order to investigate if HFO activity is an artifact caused by the evoked waveform. The peaks of stimulus pulses were detected, and the 22s of data during each stimulation was aligned with respect to the peak. A moving template was extracted using the Principal Component Analysis method over each 1s of data with 50% overlap. The largest eigenvector corresponded to the stimulus artifact and accompanying inter-pulse evoked activity. Each waveform in the aligned data was reconstructed in this way and the residual was calculated by subtraction of the reconstructed data from the original raw trace.

Statistical Analysis

Unless otherwise denoted, the comparative statistical analyses were performed using paired, two-tailed, non-parametric tests (Wilcoxon signed-rank test), given the non-normal distribution of most variables studied (Anderson-Darling test, $p<0.05$). Spearman coefficient was used for the correlation analyses. The significance of the decay of evoked activity was tested with one-tailed t-test due to the normality. The threshold alpha level to determine significance was 0.05. The circular statistics regarding phase angles were performed using Circular Statistics Toolbox [37]. On each box in the boxplots, the central mark indicates

the median, and the bottom and top edges of the box indicate the 25th and 75th percentiles, respectively. The whiskers extend to the most extreme data points not considered outliers, and the outliers are plotted individually using the '+' symbol. The individual data points are also plotted as red circles.

Acknowledgments: We would like to thank the patients for their participation. We acknowledge the OR supervisor Carolle Daniel and the rest of the operating room personnel at Baylor St Luke's Medical Center for their help in data collection and Texas Institute for Measurement, Evaluation, and Statistics (TIMES) for the resources and support they provided for our research. This research was supported by National Science Foundation Grant CBET-1343548.

Author Contributions: M.O., A.V. and N.F.I. designed research; A.V. and S.A.S. performed the surgeries; M.O. performed the data collection; M.O. and N.F.I. analyzed the data; M.O. and N.F.I. wrote the first draft; and all authors edited the paper.

Competing interests: Two provisional patents (pending) related to the biomarkers described in this manuscript have been filed by University of Houston. The inventors/contributors are the same as the manuscript authors. The application numbers are: 63/068,155 and 63/066,141.

Data availability statement: The data that support the findings of this study are available on request from the corresponding author. The raw data are not publicly available as the data might contain potentially identifying or sensitive information that could compromise the privacy of the research participants.

References

1. McIntyre, C. C. & Hahn, P. J. Network perspectives on the mechanisms of deep brain stimulation. *Neurobiol Dis* **38**, 329–337 (2010).

2. Miocinovic, S., Somayajula, S., Chitnis, S. & Vitek, J. L. History, Applications, and Mechanisms of Deep Brain Stimulation. *JAMA Neurol* **70**, 163 (2013).

3. Youngerman, B. E., Chan, A. K., Mikell, C. B., McKhann, G. M. & Sheth, S. A. A decade of emerging indications: deep brain stimulation in the United States. *J Neurosurg* **125**, 461–471 (2016).

4. Benazzouz, A. *et al.* Effect of high-frequency stimulation of the subthalamic nucleus on the neuronal activities of the substantia nigra pars reticulata and ventrolateral nucleus of the thalamus in the rat. *Neuroscience* **99**, 289–295 (2000).

5. Filali, M., Hutchison, W. D., Palter, V. N., Lozano, A. M. & Dostrovsky, J. O. Stimulation-induced inhibition of neuronal firing in human subthalamic nucleus. *Exp Brain Res* **156**, 274–281 (2004).

6. Meissner, W. *et al.* Subthalamic high frequency stimulation resets subthalamic firing and reduces abnormal oscillations. *Brain* **128**, 2372–2382 (2005).

7. Dostrovsky, J. O. *et al.* Microstimulation-Induced Inhibition of Neuronal Firing in Human Globus Pallidus. *J Neurophysiol* **84**, 570–574 (2000).

8. Welter, M.-L. *et al.* Effects of High-Frequency Stimulation on Subthalamic Neuronal Activity in Parkinsonian Patients. *Arch Neurol* **61**, 89 (2004).

9. McConnell, G. C., So, R. Q., Hilliard, J. D., Lopomo, P. & Grill, W. M. Effective Deep Brain Stimulation Suppresses Low-Frequency Network Oscillations in the Basal Ganglia by Regularizing Neural Firing Patterns. *J Neurosci* **32**, 15657–15668 (2012).

10. Hashimoto, T., Elder, C. M., Okun, M. S., Patrick, S. K. & Vitek, J. L. Stimulation of the Subthalamic Nucleus Changes the Firing Pattern of Pallidal Neurons. *J Neurosci* **23**, 1916–1923 (2003).

11. Zhuang, Q. X. *et al.* Regularizing firing patterns of rat subthalamic neurons ameliorates parkinsonian motor deficits. *J Clin Invest* **128**, 5413–5427 (2018).

12. Xu, W., Russo, G. S., Hashimoto, T., Zhang, J. & Vitek, J. L. Subthalamic Nucleus Stimulation Modulates Thalamic Neuronal Activity. *J Neurosci* **28**, 11916–11924 (2008).

13. Grill, W. M., Snyder, A. N. & Miocinovic, S. Deep brain stimulation creates an informational lesion of the stimulated nucleus. *Neuroreport* **15**, 1137–1140 (2004).

14. Johnson, M. D., Miocinovic, S., McIntyre, C. C. & Vitek, J. L. Mechanisms and targets of deep brain stimulation in movement disorders. *Neurotherapeutics* **5**, 294–308 (2008).

15. Guo, Y., Rubin, J. E., McIntyre, C. C., Vitek, J. L. & Terman, D. Thalamocortical Relay Fidelity Varies Across Subthalamic Nucleus Deep Brain Stimulation Protocols in a Data-Driven Computational Model. *J Neurophysiol* **99**, 1477–1492 (2008).

16. Rubin, J. E. & Terman, D. High Frequency Stimulation of the Subthalamic Nucleus Eliminates Pathological Thalamic Rhythmicity in a Computational Model. *J Comput Neurosci* **16**, 211–235 (2004).

17. Saenger, V. M. *et al.* Uncovering the underlying mechanisms and whole-brain dynamics of deep brain stimulation for Parkinson's disease. *Sci Rep* **7**, 9882 (2017).

18. Santaniello, S. *et al.* Therapeutic mechanisms of high-frequency stimulation in Parkinson's disease and neural restoration via loop-based reinforcement. *Proc Natl Acad Sci* **112**, E586–E595 (2015).

19. Benabid, A. L., Chabardes, S., Mitrofanis, J. & Pollak, P. Deep brain stimulation of the subthalamic nucleus for the treatment of Parkinson's disease. *Lancet Neurol* 67–81 (2009).

20. Gross, R. E., Krack, P., Rodriguez-Oroz, M. C., Rezai, A. R. & Benabid, A.-L. Electrophysiological mapping for the implantation of deep brain stimulators for Parkinson's disease and tremor. *Mov Disord* **21**, S259–S283 (2006).

21. Oswal, A., Brown, P. & Litvak, V. Synchronized neural oscillations and the pathophysiology of Parkinson's disease. *Curr Opin Neurol* **26**, 662–670 (2013).

22. Brittain, J.-S. & Brown, P. Oscillations and the basal ganglia: Motor control and beyond. *Neuroimage* **85**, 637–647 (2014).

23. Brown, P. *et al.* Effects of stimulation of the subthalamic area on oscillatory pallidal activity in Parkinson's disease. *Exp Neurol* **188**, 480–490 (2004).

24. Eusebio, A. *et al.* Deep brain stimulation can suppress pathological synchronisation in parkinsonian patients. *J Neurol Neurosurg Psychiatry* **82**, 569–573 (2011).

25. Priori, A. *et al.* Rhythm-specific pharmacological modulation of subthalamic activity in Parkinson's disease. *Exp Neurol* **189**, 369–379 (2004).

26. Weinberger, M. *et al.* Beta Oscillatory Activity in the Subthalamic Nucleus and Its Relation to Dopaminergic Response in Parkinson's Disease. *J Neurophysiol* **96**, 3248–3256 (2006).

27. Hoang, K. B. & Turner, D. A. The Emerging Role of Biomarkers in Adaptive Modulation of Clinical Brain Stimulation. *Neurosurgery* **85**, E430–E439 (2019).

28. Swann, N. C. *et al.* Gamma Oscillations in the Hyperkinetic State Detected with Chronic Human Brain Recordings in Parkinson's Disease. *J Neurosci* **36**, 6445–6458 (2016).

29. Ozturk, M. *et al.* Distinct subthalamic coupling in the ON state describes motor performance in Parkinson's disease. *Mov Disord* (2019). doi:10.1002/mds.27800

30. Özkurt, T. E. *et al.* High frequency oscillations in the subthalamic nucleus: A neurophysiological marker of the motor state in Parkinson's disease. *Exp Neurol* **229**, 324–331 (2011).

31. Foffani, G. *et al.* 300-Hz subthalamic oscillations in Parkinson's disease. *Brain* **126**, 2153–2163 (2003).

32. Lopez-Azcarate, J. *et al.* Coupling between beta and high-frequency activity in the human subthalamic nucleus may be a pathophysiological mechanism in Parkinson's disease. *J Neurosci* **30**, 6667–6677 (2010).

33. van Wijk, B. C. M. *et al.* Subthalamic nucleus phase-amplitude coupling correlates with motor impairment in Parkinson's disease. *Clin Neurophysiol* **127**, 2010–2019 (2016).

34. Zhou, A., Johnson, B. C. & Muller, R. Toward true closed-loop neuromodulation: artifact-free recording during stimulation. *Curr Opin Neurobiol* **50**, 119–127 (2018).

35. Telkes, I., Jimenez-Shahed, J., Viswanathan, A., Abosch, A. & Ince, N. F. Prediction of STN-DBS Electrode Implantation Track in Parkinson's Disease by Using Local Field Potentials. *Front Neurosci* **10**, 1–16 (2016).

36. Ozturk, M. *et al.* Randomized, Double-Blind Assessment of LFP Versus SUA Guidance in STN-DBS Lead Implantation: A Pilot Study. *Front Neurosci* **14**, (2020).

37. Berens, P. CircStat : A MATLAB Toolbox for Circular Statistics. *J Stat Softw* **31**, 293–295 (2009).

38. Stypulkowski, P. H., Giftakis, J. E. & Billstrom, T. M. Development of a Large Animal Model for Investigation of Deep Brain Stimulation for Epilepsy. *Stereotact Funct Neurosurg* **89**, 111–122 (2011).

39. Kent, A. R. *et al.* Measurement of Evoked Potentials During Thalamic Deep Brain Stimulation. *Brain Stimul* **8**, 42–56 (2015).

40. Parker, J. L. *et al.* Evoked Compound Action Potentials Reveal Spinal Cord Dorsal Column Neuroanatomy. *Neuromodulation Technol Neural Interface* **23**, 82–95 (2020).

41. Ashby, P. *et al.* Potentials recorded at the scalp by stimulation near the human subthalamic nucleus. *Clin Neurophysiol* **112**, 431–437 (2001).

42. Gmel, G. E. *et al.* A new biomarker for subthalamic deep brain stimulation for patients with advanced Parkinson's disease - A pilot study. *J Neural Eng* **12**, (2015).

43. Sinclair, N. C. *et al.* Subthalamic nucleus deep brain stimulation evokes resonant neural activity. *Ann Neurol* **83**, 1027–1031 (2018).

44. Sinclair, N. C. *et al.* Deep brain stimulation for Parkinson's disease modulates high-frequency evoked and spontaneous neural activity. *Neurobiol Dis* **130**, 104522 (2019).

45. Li, S., Arbuthnott, G. W., Jutras, M. J., Goldberg, J. A. & Jaeger, D. Resonant Antidromic Cortical Circuit Activation as a Consequence of High-Frequency Subthalamic Deep-Brain Stimulation. *J Neurophysiol* **98**, 3525–3537 (2007).

46. Miocinovic, S. *et al.* Cortical Potentials Evoked by Subthalamic Stimulation Demonstrate a Short Latency Hyperdirect Pathway in Humans. *J Neurosci* **38**, 9129–9141 (2018).

47. Moran, A., Stein, E., Tischler, H., Belelovsky, K. & Bar-Gad, I. Dynamic Stereotypic Responses of Basal Ganglia Neurons to Subthalamic Nucleus High-Frequency Stimulation in the Parkinsonian Primate. *Front Syst Neurosci* **5**, 1–11 (2011).

48. Montgomery, E. B. & Gale, J. T. Mechanisms of action of deep brain stimulation (DBS). *Neurosci Biobehav Rev* **32**, 388–407 (2008).

49. Wichmann, T. & DeLong, M. R. Basal ganglia discharge abnormalities in Parkinson's disease. in *Parkinson's Disease and Related Disorders* 21–25 (Springer Vienna, 2006). doi:10.1007/978-3-211-45295-0_5

50. Herrington, T. M., Cheng, J. J. & Eskandar, E. N. Mechanisms of deep brain stimulation. *J Neurophysiol* **115**, 19–38 (2016).

51. Montgomery, E. Dynamically Coupled, High-Frequency Reentrant, Non-linear Oscillators Embedded in Scale-Free Basal Ganglia-Thalamic-Cortical Networks Mediating Function and Deep Brain Stimulation Efiects. *Nonlinear Stud* **11**, (2004).

52. Huang, H., Watts, R. L. & Montgomery, E. B. Effects of deep brain stimulation frequency on bradykinesia of Parkinson's disease. *Mov Disord* **29**, 203–206 (2014).

53. Cleary, D. R. *et al.* Deep brain stimulation entrains local neuronal firing in human globus pallidus internus. *J Neurophysiol* **109**, 978–987 (2013).

54. Montgomery, Jr, E. B. & Gale, J. T. Neurophysiology and Neurocircuitry. in *Handbook of Parkinson's Disease* (eds. Pahwa, R. & Lyons, K. E.) 223–238 (CRC Press, 2007).

55. Garcia, L., D'Alessandro, G., Fernagut, P., Bioulac, B. & Hammond, C. Impact of High-Frequency Stimulation Parameters on the Pattern of Discharge of Subthalamic Neurons. *J Neurophysiol* **94**, 3662–3669 (2005).

56. Garcia, L., D'Alessandro, G., Bioulac, B. & Hammond, C. High-frequency stimulation in Parkinson's disease: more or less? *Trends Neurosci* **28**, 209–216 (2005).

57. Bevan, M. D., Magill, P. J., Terman, D., Bolam, J. P. & Wilson, C. J. Move to the rhythm: oscillations in the subthalamic nucleus-external globus pallidus network. *Trends Neurosci* **25**, 525–31 (2002).

58. Mastro, K. J. & Gittis, A. H. Striking the right balance: Cortical modulation of the subthalamic nucleus-globus pallidus circuit. *Neuron* **85**, 233–235 (2015).

59. Montgomery, E. B. Deep Brain Stimulation: Mechanisms of Action. in *Neurostimulation* 1–19 (John Wiley & Sons, Ltd, 2013). doi:10.1002/9781118346396.ch1

60. Kita, H. & Kitai, S. T. Intracellular study of rat globus pallidus neurons: membrane properties and responses to neostriatal, subthalamic and nigral stimulation. *Brain Res* **564**, 296–305 (1991).

61. Escobar, D. *et al.* Parkinsonism and Vigilance: Alteration in neural oscillatory activity and phase-amplitude coupling in the basal ganglia and motor cortex. *J Neurophysiol* **118**, jn.00388.2017 (2017).

62. Bergman, H., Wichmann, T., Karmon, B. & DeLong, M. R. The primate subthalamic nucleus. II. Neuronal activity in the MPTP model of parkinsonism. *J Neurophysiol* **72**, 507–20 (1994).

63. Soares, J. *et al.* Role of External Pallidal Segment in Primate Parkinsonism: Comparison of the Effects of 1-Methyl-4-Phenyl-1,2,3,6-Tetrahydropyridine-Induced Parkinsonism and Lesions of the External Pallidal Segment. *J Neurosci* **24**, 6417–6426 (2004).

64. Hahn, P. J. *et al.* Pallidal burst activity during therapeutic deep brain stimulation. *Exp Neurol* **211**, 243–251 (2008).

65. Li, Q. *et al.* Therapeutic Deep Brain Stimulation in Parkinsonian Rats Directly Influences Motor Cortex. *Neuron* **76**, 1030–1041 (2012).

66. Ozturk, M. *et al.* Subthalamic Single Cell and Oscillatory Neural Dynamics of a Dyskinetic Medicated Patient With Parkinson's Disease. *Front Neurosci* **14**, 1–8 (2020).

67. Kaku, H. *et al.* Unsupervised clustering reveals spatially varying single neuronal firing patterns in the subthalamic nucleus of patients with Parkinson's disease. *Clin Park Relat Disord* **3**, 100032 (2020).

68. Sharott, A. *et al.* Activity Parameters of Subthalamic Nucleus Neurons Selectively Predict Motor Symptom Severity in Parkinson's Disease. *J Neurosci* **34**, 6273–6285 (2014).

69. Reese, R. *et al.* Subthalamic deep brain stimulation increases pallidal firing rate and regularity. *Exp Neurol* **229**, 517–521 (2011).

70. Erwin, B., Jr, M. M. & Baker, K. K. Mechanisms of deep brain stimulation and future technical developments. *Neurol Res* **22**, 259–266 (2000).

71. Foffani, G. *et al.* Subthalamic oscillatory activities at beta or higher frequency do not change after high-frequency DBS in Parkinson's disease. *Brain Res Bull* **69**, 123–130 (2006).

72. Montgomery, E. B., Gale, J. T. & Huang, H. Methods for isolating extracellular action potentials and removing stimulus artifacts from microelectrode recordings of neurons requiring minimal operator intervention. *J Neurosci Methods* **144**, 107–125 (2005).

73. Stefani, A. *et al.* The clinical efficacy of L-DOPA and STN-DBS share a common marker: Reduced GABA content in the motor thalamus. *Cell Death Dis* **2**, 1–9 (2011).

74. Rizzone, M. *et al.* Deep brain stimulation of the subthalamic nucleus in Parkinson's disease: effects of variation in stimulation parameters. *J Neurol Neurosurg Psychiatry* **71**, 215–9 (2001).

75. Moro, E. *et al.* The impact on Parkinson's disease of electrical parameter settings in STN stimulation. *Neurology* **59**, 706–713 (2002).

76. Fogelson, N. *et al.* Frequency dependent effects of subthalamic nucleus stimulation in Parkinson's disease. *Neurosci Lett* **382**, 5–9 (2005).

77. Eusebio, A. *et al.* Effects of low-frequency stimulation of the subthalamic nucleus on movement in Parkinson's disease. *Exp Neurol* **209**, 125–130 (2008).

78. Agnesi, F., Connolly, A. T., Baker, K. B., Vitek, J. L. & Johnson, M. D. Deep Brain Stimulation Imposes Complex Informational Lesions. *PLoS One* **8**, 1–11 (2013).

79. Kuncel, A. M., Cooper, S. E., Wolgamuth, B. R. & Grill, W. M. Amplitude- and Frequency-Dependent Changes in Neuronal Regularity Parallel Changes in Tremor With Thalamic Deep Brain Stimulation. *IEEE Trans Neural Syst Rehabil Eng* **15**, 190–197 (2007).

80. Kühn, A. A. *et al.* High-Frequency Stimulation of the Subthalamic Nucleus Suppresses Oscillatory Activity in Patients with Parkinson's Disease in Parallel with Improvement in Motor Performance. *J Neurosci* **28**, 6165–6173 (2008).

81. Kane, A., Hutchison, W. D., Hodaie, M., Lozano, A. M. & Dostrovsky, J. O. Dopamine-dependent high-frequency oscillatory activity in thalamus and subthalamic nucleus of patients with Parkinson's disease. *Neuroreport* **20**, 1549–1553 (2009).

82. Kühn, A. A. *et al.* Event-related beta desynchronization in human subthalamic nucleus correlates with motor performance. *Brain* **127**, 735–746 (2004).

83. Litvak, V. *et al.* Movement-related changes in local and long-range synchronization in parkinson's disease revealed by simultaneous magnetoencephalography and intracranial recordings. *J Neurosci* **32**, 10541–10553 (2012).

84. Thompson, J. A. *et al.* Sleep patterns in Parkinson's disease: direct recordings from the subthalamic nucleus. *J Neurol Neurosurg Psychiatry* **89**, 95–104 (2018).

85. Urrestarazu, E. *et al.* Beta activity in the subthalamic nucleus during sleep in patients with Parkinson's disease. *Mov Disord* **24**, 254–260 (2009).

86. Leventhal, D. K. *et al.* Basal ganglia beta oscillations accompany cue utilization. *Neuron* **73**, 523–536 (2012).

87. Orfanidis, S. J. *Introduction to signal processing*. (Prentice-Hall, Inc., 1995).

Figures

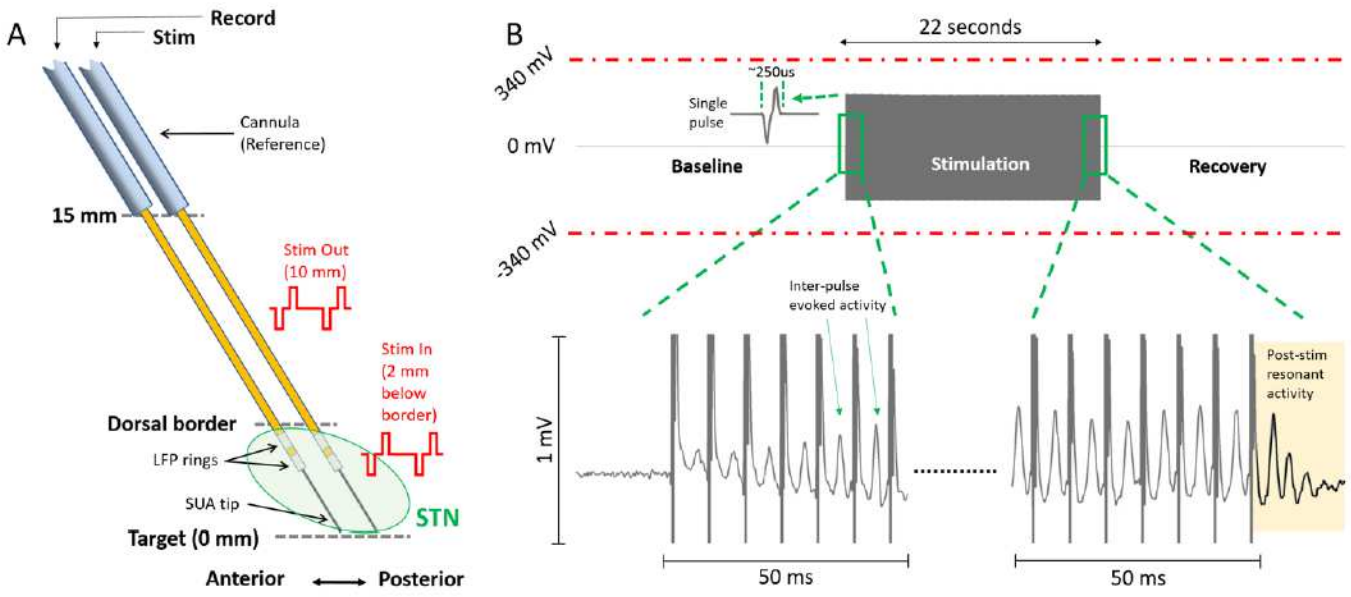

Figure 1

Experimental paradigm and sample stimulation segment showing that LFP recordings did not saturate with the high input range of the amplifier. (A) The microelectrode diagrams depicting the recording and stimulating electrodes. The “out-STN” stimulation was performed 10mm above the ventral border of the STN. Bipolar microelectrodes with two 0.5mm wide stainless steel rings separated by 0.5mm were used to deliver biphasic electrical stimulation and record LFP activity. The “in-STN” stimulation experiments were performed 2mm below the dorsal border of the STN, characterized by the increased background activity and neuronal spiking recorded from the fine microelectrode tip. (B) Sample 66s raw LFP recording illustrates that the amplifier was not saturated during stimulation of the other electrode. Single pulse waveform illustrates that the biphasic stimulation pulse was captured within a short time, allowing the LFP recordings to continue with minimal interruption. Zoomed 50ms segments from beginning and the end shows evoked potentials induced with each stimulus pulse. The evoked waveform amplitude increases with each pulse and settles after ~10 pulses. With the termination of the stimulation, the resonance in the evoked activity can be observed longer, which dampens within 20ms.

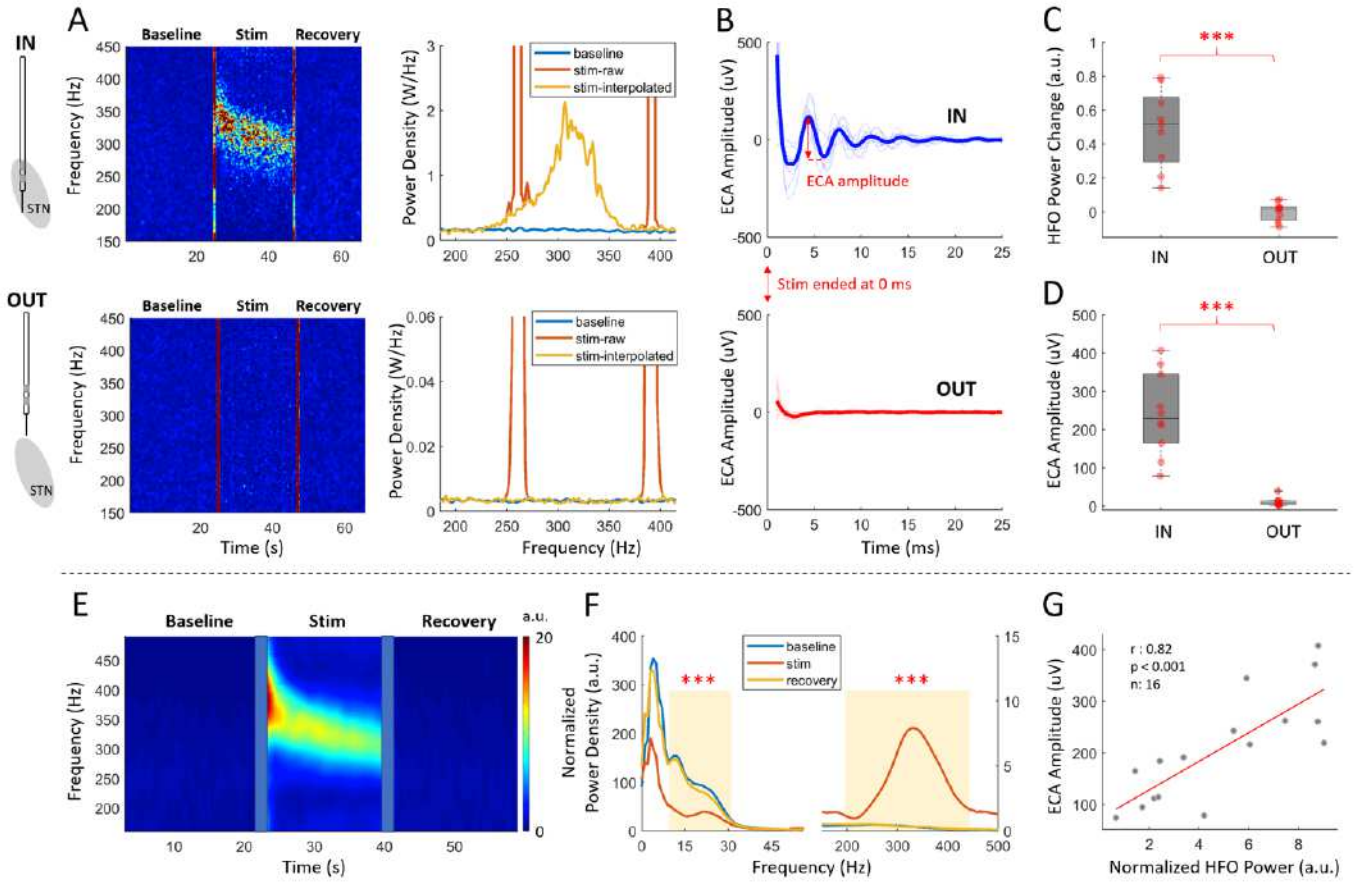

Figure 2

HFO and resonant evoked compound activity are observed during high-frequency DBS only in the STN. In 10 hemispheres, 130Hz stimulation was performed out- and in-STN to identify and eliminate the artifacts caused by the stimulation or the recording hardware. (A) Representative TFM and PSD plots of out- and in-STN stimulation from a sample patient shows that HFO was induced only within the STN. The vertical red lines on TFMs are the transition artifacts associated with turning the stimulator on and off. The large artifacts caused by harmonics of the stimulation frequency are interpolated. The color scale of the TFMs are the same as the limits of the y-axis of their respective PSD plots. (B) The evoked response at the end of 22s stimulation was only seen in-STN. The thick lines illustrate the mean waveform. The first 1ms after the stimulation pulse is blanked out due to large artifact amplitude. (C) Comparison of the HFO power change between out- and in-STN stimulations show a significant difference (n=10). (D) Similarly, the difference between ECA amplitude of out- and in-STN stimulations was significant (n=10). (E) The grand average TFM from all 16 hemispheres with 130 Hz in-STN stimulation shows a stark enhancement in the HFO range, similar to the representative subject. The transition artifacts on TFM are masked with blue boxes. (F) The grand average PSD plots for baseline, stimulation and recovery periods from all 16 hemispheres with high frequency stimulation in-STN. There was a significant suppression in the beta and significant enhancement in the HFO ranges (n=16). (G) In the STN, the ECA amplitude and induced HFO power correlated (n=16). *** denotes significance <0.001

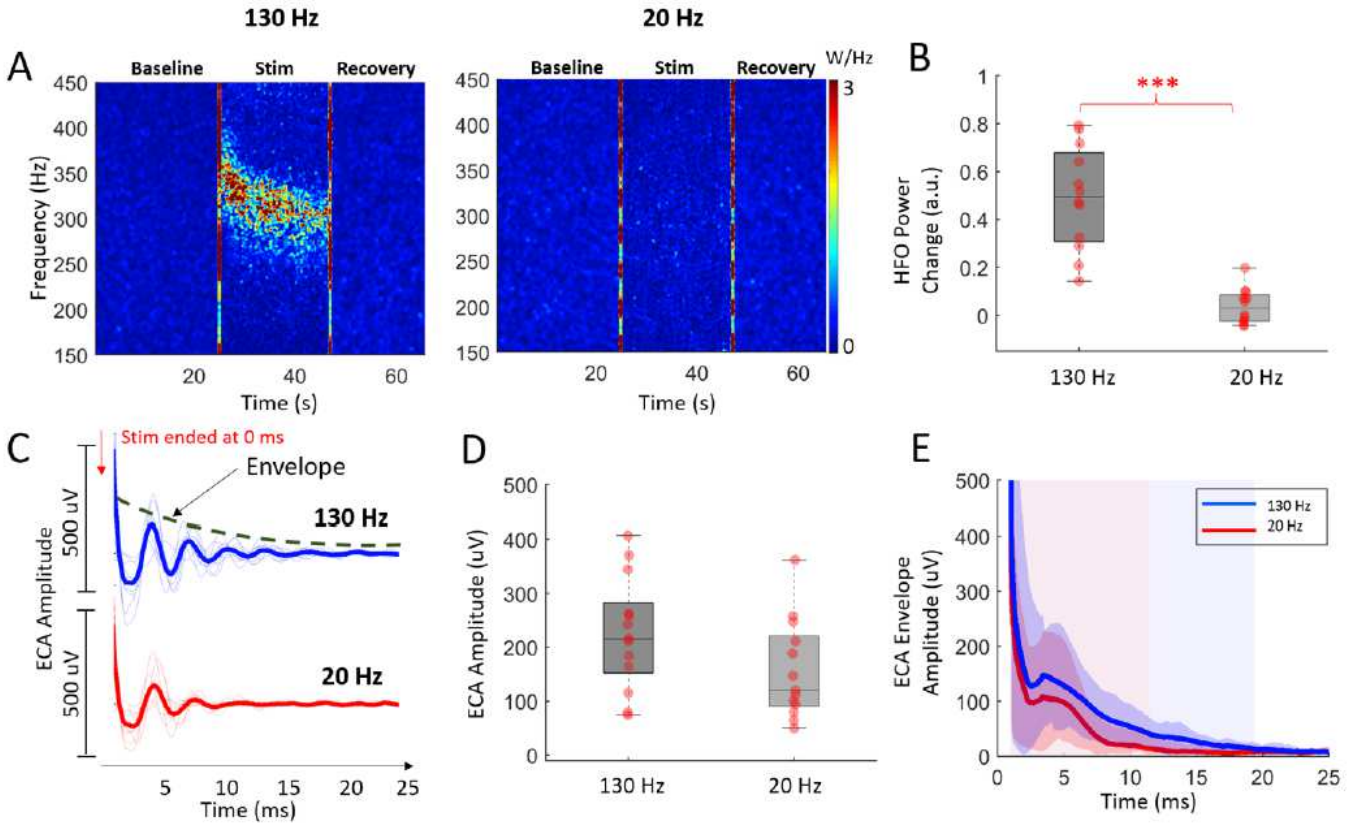

Figure 3

Low-frequency DBS does not induce HFO but evokes compound activity that damped faster. (A) Representative TFMs of high- and low- frequency stimulation from a patient shows that HFO was induced only with the former. The large artifacts caused by harmonics of the stimulation frequency are interpolated. The vertical red lines on TFMs are the transition artifacts associated with turning the stimulator on and off. (B) The HFO power change was significantly higher with high-frequency stimulation (n=13). (C) Both high- and low- frequency stimulation induced ECA. The first 1ms after the stimulation pulse is omitted due to large artifact amplitude. (D) The difference between ECA amplitude after high- and low-frequency stimulation was only marginally significant (n=13). (E) The dampening of ECA derived from the envelope of the Hilbert transform of the waveforms was significantly faster after low-frequency stimulation (19ms vs 11ms, n=13). *** denotes significance <0.001.

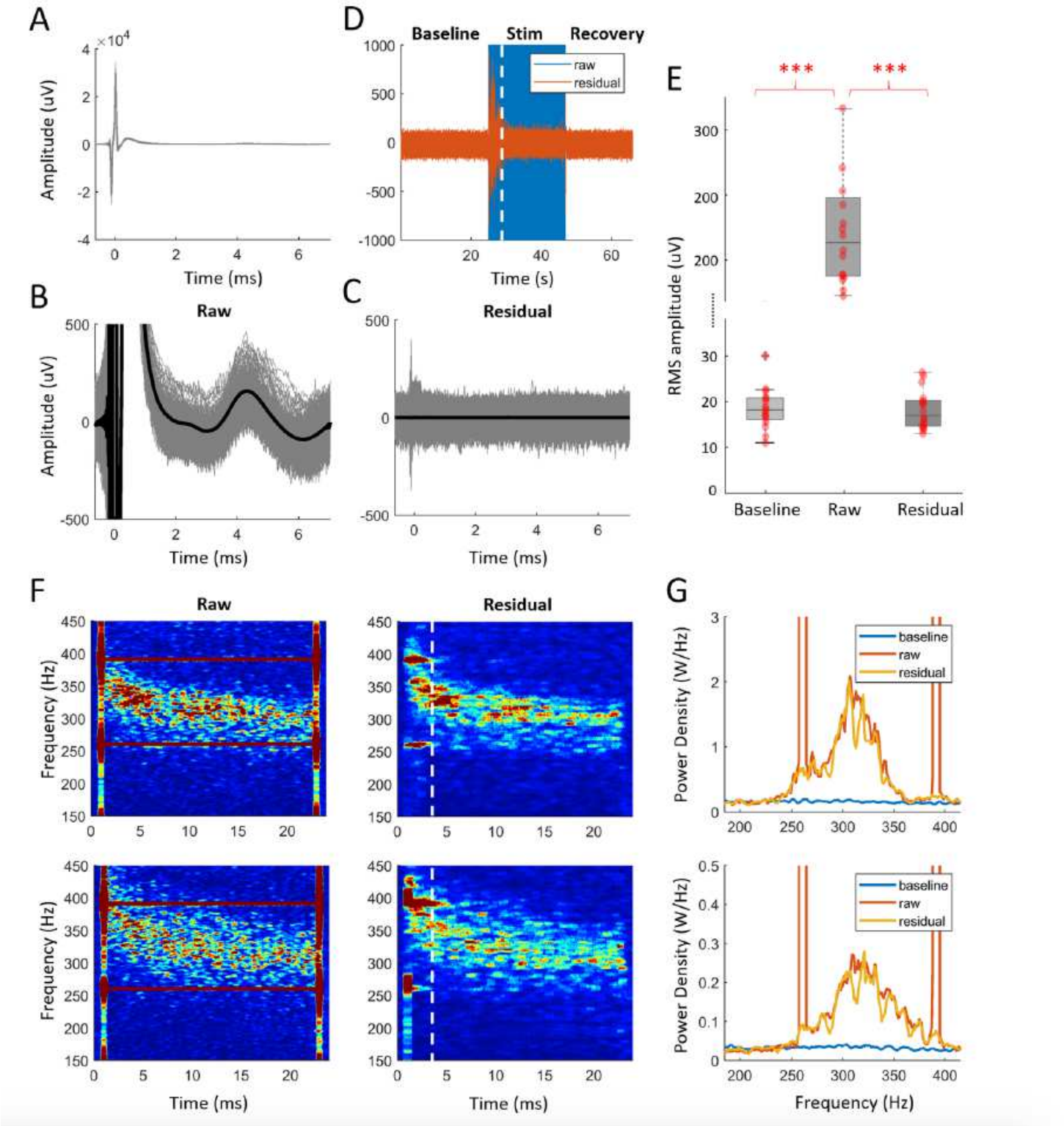

Figure 4

HFO induced by therapeutic 130 Hz DBS is present even after removal of evoked waveform between stimulation pulses. (A) The overlay plot of raw data aligned with respect to the stimulus pulses (0.5ms pre-onset was used to avoid edge artifacts). The large biphasic stimulation artifact at 0ms masks both ECA and other LFP activity. (B, C) The same segment in A shown with 1mV amplitude scale before and after denoising, to better demonstrate the removal of ECA waveform between pulses (thicker lines

indicate the average waveform). The residual was obtained by subtraction of reconstructed segments from the raw data and it is devoid of stimulus pulse and inter-pulse evoked activity. (D) The amplitude range of the denoised (residual) data is similar to the baseline levels, except the first 3s seconds of transient period. This segment, denoted with the dashed lines, was removed from overlay plots for clarity and excluded from bandpower calculations as well. (E) The root-mean-square (RMS) amplitude of the baseline segment before stimulation as well as raw and residual traces during stimulation. There was no significant difference between baseline and the denoised stimulation segment (n=16). The first 1ms including the large stimulation artifact was omitted from the RMS calculations to capture the amplitude levels associated with the evoked response. (F) TFM of the raw and residual segments and (G) their PSD plots from two representative patients illustrate that the denoising primarily removes the artifacts at the harmonics of stimulation frequency while keeping the enhanced HFO intact. The color scale of the TFMs are same as limits of y-axis of their corresponding PSD plots. The dashed lines on TFMs denote the transition artifacts associated with turning the stimulator on and off. *** denotes significance <0.001

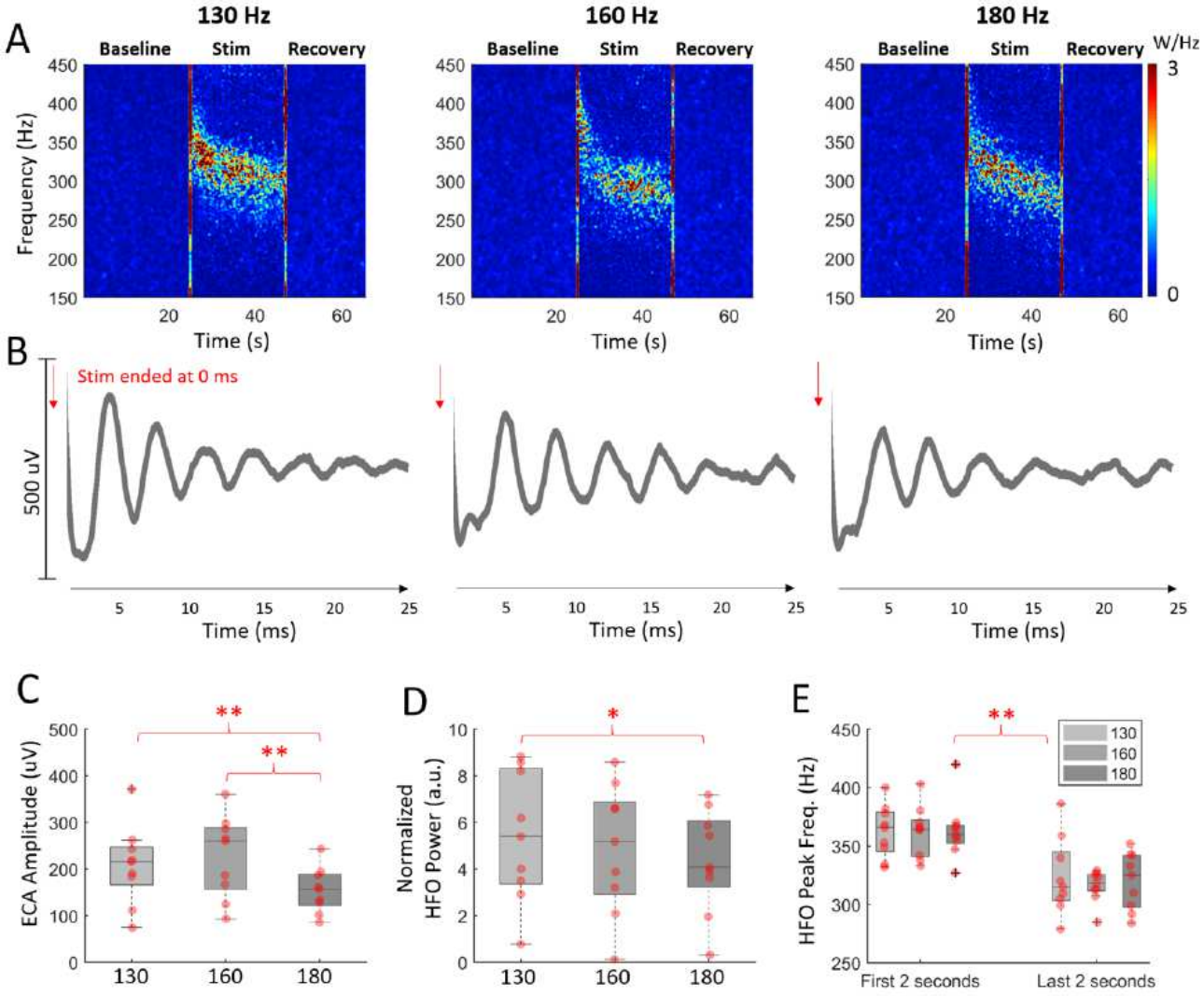

Figure 5

High-frequency stimulations modulate HFO and ECA in different amplitudes. (A) The HFO was enhanced with all stimulation frequencies. The large artifacts caused by harmonics of the stimulation frequency are interpolated. The vertical red lines on TFMs are the transition artifacts associated with turning the stimulator on and off. (B) The ECA waveform after 22s stimulation period was resonant after all high-frequency stimulations. The first 1ms after the stimulation pulse is omitted due to large artifact amplitude. (C) The comparison ECA amplitude after 22s of stimulation showed that ECA after 180 Hz stimulation was significantly smaller (n=9). (D) The induced HFO bandpowers were only significantly different between 130 and 180 Hz groups (n=9). (E) The peak frequency of HFO in the first and last two seconds of stimulation were significantly different in all groups (n=9) but not different between groups. ** denotes significance <0.01, * denotes significance <0.05

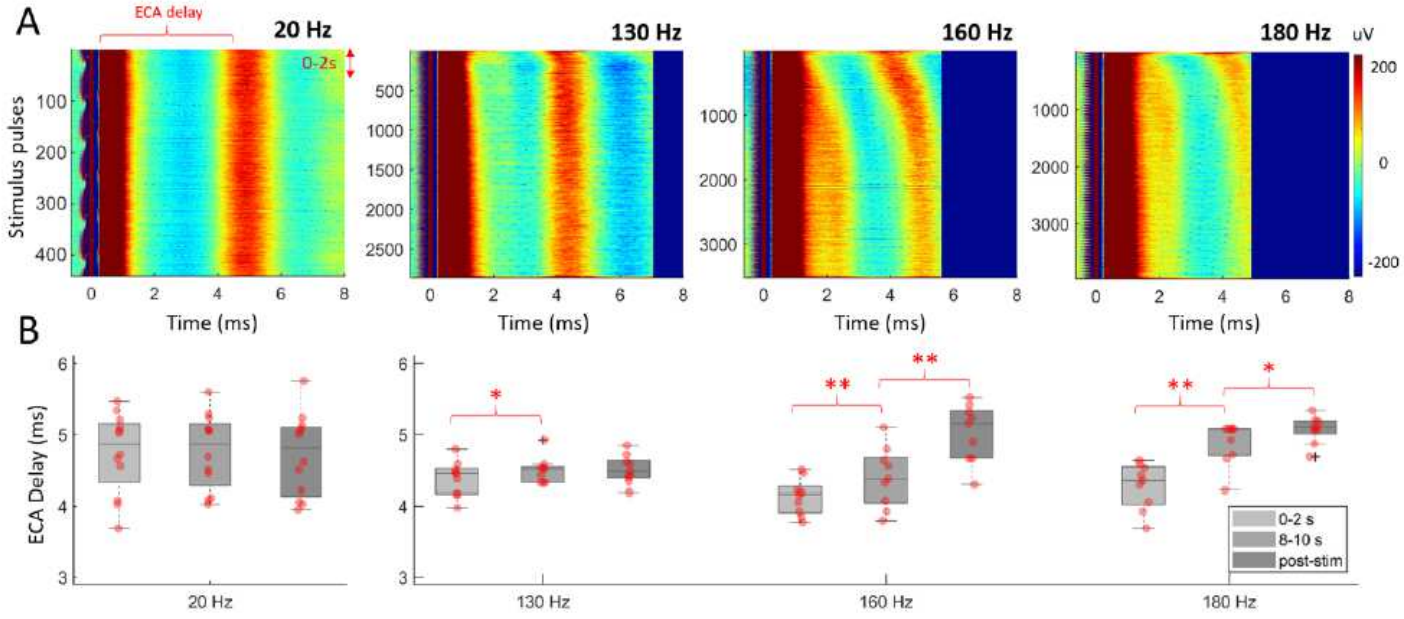

Figure 6

Inter-pulse evoked activity shows adaptation only with high-frequency stimulation. (A) The representative aligned raw data with respect to the stimulus pulse for 130, 160, 180 and 20 Hz stimulation (0.5ms pre-onset, up to 8ms is shown). (B) The ECA delay comparison in the 0-2s, 8-10s and after 22s demonstrate the differences in adaptation between 130, 160, 180 (n=9) and 20 Hz (n=13) stimulations. The ECA delay, which denotes the delay of the first evoked peak, was consistent throughout the 20 Hz stimulation period, indicating no adaptation. The fastest adaptation was with 130 Hz, settling after 2s. ** denotes significance <0.01, * denotes significance <0.05.

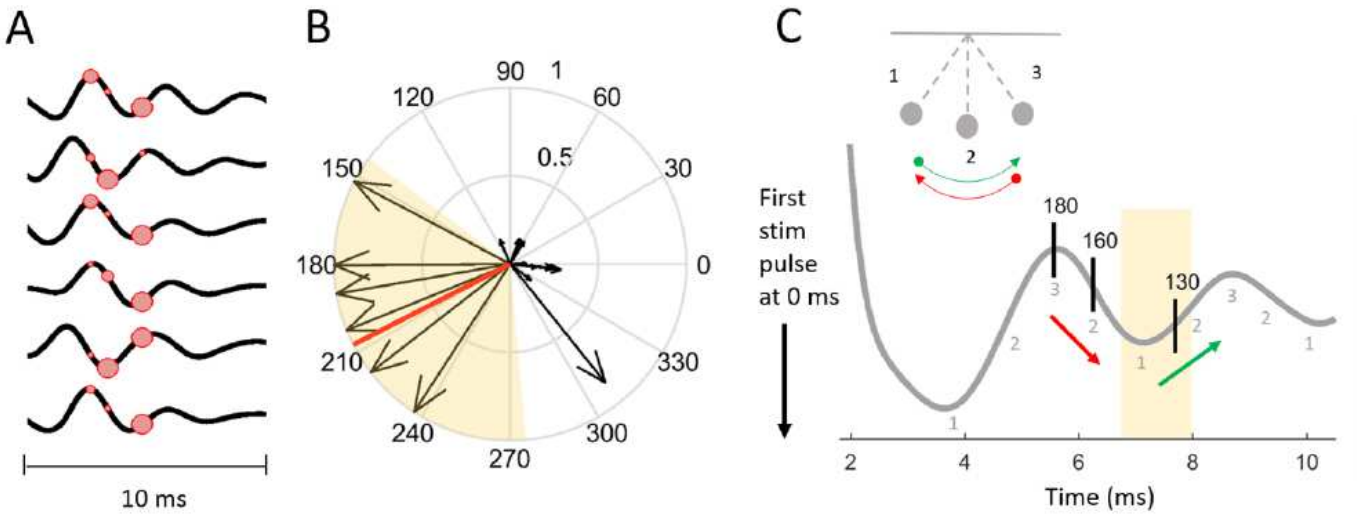

Figure 7

The DBS can be tuned to provide maximum modulatory effect based on the phase of ECA waveform. (A) The ECA waveforms after 22s of low-frequency stimulation from the six subjects with both 20 Hz and high-frequency stimulation experiments. The location of the red circles denotes where the next 130, 160 and 180 Hz stimulation pulses would be, if the stimulation continued with the specified frequency. The size of the circle denotes the relative amplitude of the induced HFO by that stimulation. (B) The information in A is presented on polar coordinates to illustrate the phase preference. The arrow length denotes the relative amplitude of the induced HFO power. The mean angle was 208 degrees and is denoted by the red line. The preferred phase was between 143-275 degrees (n=6) and is denoted by the highlighted background. (C) A pendulum and a representative ECA waveform to illustrate the swing-like behavior of the evoked response. The numbers indicate the positions of pendulum. The shaded region illustrates the preferred phase angles from B. When the next stimulation pulse is at a preferred phase location (forward motion, green), the modulatory effects can be enhanced. On the other hand, stimulating at the other phase (backward motion, red) could hinder effect of DBS.

Supplementary Files

This is a list of supplementary files associated with this preprint. Click to download.

- ElectroceuticalHFOECAsupp.pdf